UNIVERSITÀ DEGLI STUDI DI MILANO

FACULTY OF MEDICINE AND SURGERY

DOCTORAL PROGRAM IN

TRANSLATIONAL MEDICINE

XXXVII CYCLE

DEPARTMENT OF "***Clinical Sciences and Community Health***"

DOCTORAL THESIS entitled

Elucidating the Role of HET0016 in ameliorating 20-HETE Induced Oxidative Stress and Liver Injury in β-Thalassemia: A Novel Therapeutic Target

PhD Candidate

Rayan BOU FAKHREDIN

Matriculation N° R13252

TUTOR: **Prof. Irene MOTTA**

CO-TUTOR: **Prof. Flora PEYVANDI**

PhD PROGRAM COORDINATOR: **Prof. Chiarella SFORZA**

Academic Year 2023-2024

ABSTRACT

Background: Reactive oxygen species (ROS) are one of the main contributors to pathological outcomes in β-thalassemia, with their generation being a consequence of iron overload and abnormal red blood cell metabolism. We have previously shown that CYP450 mediates ROS production in the liver of a mouse model of β-thalassemia through an increase in 20-hydroxyeicosatetraenoic acid (20-HETE) activity.

Aim: The aim of this study is to assess the efficacy of N-Hydroxy-N'-(4-butyl-2-methylphenyl)-formamidine (HET0016), an inhibitor of 20-HETE formation, in reducing 20-HETE-mediated oxidative stress and injury in the livers of mice affected by β-thalassemia.

Methods: $Hbb^{th3/+}$ mice (The Jackson Laboratory) were used as a model of non-transfusion dependent thalassemia (NTDT) and were divided into 3 groups: a control group (N=11) treated intraperitoneally (IP) with a 1:1 solution of dimethyl sulfoxide (DMSO) and phosphate-buffered saline (PBS), $Hbb^{th3/+}$ mice treated with a 1:1 solution of DMSO and PBS (N=14), and $Hbb^{th3/+}$ mice treated with HET0016 (N=7). HET0016 was administered in the form of a daily IP injection at a dose of 5mg/kg/day for a total duration of four weeks. Enzymatic activity of NADPH oxidases was assessed using the NADPH oxidase assay. mRNA expression levels of two isoforms of CYP4A, as well as CYP4A protein levels, were measured in the liver using Real-time Polymerase Chain Reaction (PCR) and western blot, respectively. Degree of expression of CYP4A was also evaluated in the liver by immunohistochemistry (IHC). Formalin-fixed paraffin-embedded liver tissues were also sectioned and stained with Pearl's Prussian blue stain to detect ferric iron (Fe^{3+}). Sirius red stain and measurement of hepatocyte growth factor (HGF) mRNA

expression levels were performed to detect signs of liver injury. To assess the degree of lipid peroxidation, an IHC staining for 4-hydroxynonenal (4-HNE) in addition to a malondialdehyde (MDA) colorimetric assay was performed. IHC staining for Caspase-3 was conducted to assess apoptosis. Finally, the effects of 20-HETE inhibition on the ferroptosis pathway were examined by measuring the mRNA and protein expression levels of glutathione peroxidase 4 (GPX4) in addition to measuring total glutathione (GSH) levels.

Results: In $Hbb^{th3/+}$ mice, there was an increase in intracellular ROS levels and NADPH oxidase enzymatic activity. At both mRNA level and protein level, in addition to IHC staining, a significant increase was observed in the expression of CYP4A in $Hbb^{th3/+}$ mice compared to control. This significantly decreased after HET0016 administration. Moreover, $Hbb^{th3/+}$ mice showed an increase in the lipid peroxidation markers MDA and 4-HNE, which decreased after HET0016 administration. HET0016 also ameliorated liver injury in $Hbb^{th3/+}$ mice treated with HET0016 as shown by a significant decrease in HGF mRNA expression levels and collagen fiber content. Increased tissue iron levels were detected in the liver of $Hbb^{th3/+}$ mice compared to controls and this decreased with HET0016 administration. Caspase 3 levels also decreased following treatment with HET0016. Finally, HET0016 treated $Hbb^{th3/+}$ mice showed a significant increase in GPX4 at both mRNA and protein level in addition to increased GSH levels, when compared to their non-treated counterparts.

Conclusion: Our preclinical study is the first to assess the efficacy of HET0016 in reducing 20-HETE-mediated oxidative stress and injury in the livers of mice affected by β-thalassemia. These findings lay the groundwork for future and further investigations on the role of 20-HETE induced

oxidative stress in β-thalassemia and may pave the way for a new novel therapeutic target in the field.

ACKNOWLEDGEMENT

I would first like to express my heartfelt gratitude to Prof. Irene Motta for her unwavering support over the past three years. I am deeply thankful for the warm welcome she extended to me in Milan and for her constant presence by my side. As my tutor, Prof. Motta provided invaluable guidance and created numerous opportunities for me to develop both intellectually and professionally. She always encouraged me to think independently, never imposing her opinions, but helping me recognize, evaluate, and pursue potential opportunities on my own. Over time, she has become not only my tutor and supervisor but also a friend and colleague. I am confident that under her leadership, the work in both the clinics and the lab will continue to thrive. I would also like to thank all the faculty, staff and colleagues in the clinic at Regina Elena and in the lab in Via Pace for their support throughout the years. It has been a pleasure getting to know them all.

I would also like to take this opportunity to thank my co-tutor, Prof. Flora Peyvandi, who is a true role model and an inspiration to many, including myself.

Further extending my thanks, I am sincerely grateful to Prof. Stefano Rivella from the University of Pennsylvania (UPenn) and the Children's Hospital of Philadelphia (CHOP) for his mentorship and strong support for my project. His willingness to collaborate with me and offer me the opportunity to visit and work in his lab was invaluable. My time in the Rivella lab was incredibly inspiring, and I was deeply impressed by the work they are doing. It was a privilege to interact with the lab members there and experience the positive, and collaborative atmosphere they have fostered.

Additionally, I am grateful to Prof. Assaad Eid from the Department of Anatomy, Cell Biology, and Physiological Sciences for his expert opinion, advice and support on this project. I also want to thank the members of Prof. Eid's lab, who have continued to stay in touch with me and provided invaluable assistance throughout my research.

A special note of gratitude goes to my mentors, Prof. Ali Taher and Prof. Maria Domenica Cappellini, whose continuous support has been essential to my growth and maturity. They are not only my role models in life but also a true source of inspiration. Their unwavering belief in me and their constant support have been pillars throughout my journey. I will forever be thankful for all the opportunities they provided me with to shape myself and for empowering me to embody the qualities of a future leader. They have made me not only a better scientist but also a better person. Beyond academic guidance, they have shown me the importance of leadership, creativity, work ethics, and passion in both professional and personal life. I will forever carry the lessons they have imparted to me and strive to honor them and their mentorship in all what I do moving forward in my life.

I would also like to express my gratitude to Dr. Alessandro Matte, the thesis reviewer, for his constructive feedback on my work, and to all the members of the thesis committee for their time and insights.

Finally, I am deeply thankful to my family, relatives, and friends for their unconditional love and support throughout this journey. Their constant encouragement and presence have been my foundation, providing the strength and motivation to persevere and never give up throughout the past years.

TABLE OF CONTENTS

ILLUSTRATIONS

Figures Page

TABLES

Tables Page

ABBREVIATIONS

TDT	Transfusion Dependent Thalassemia
NTDT	Non-Transfusion Dependent Thalassemia
RBC	Red blood cell
MRI	Magnetic Resonance Imaging
ERFE	Erythroferrone
GDF15	Growth differentiation factor 15
TWSG1	Twisted gastrulation 1
HCC	Hepatocellular carcinoma
ROS	Reactive Oxygen Species
HBV	Hepatitis B virus
HCV	Hepatitis C virus
GDF11	Growth differentiation factor 11
TGF-β	Transforming growth factor beta
PS	Phosphatidylserine
HIF	Hypoxia-inducible factor
PDK1	Pyruvate dehydrogenase kinase 1
NTBI	Non-transferrin-bound iron
LPI	Labile plasma iron
NADPH	Nicotinamide adenine dinucleotide phosphate
CYP450	Cytochrome P450
NOS	Nitric oxide synthase
COX	Cyclooxygenases
LIPOX	Lipoxygenases
PUFA	Polyunsaturated fatty acid
AA	Arachidonic acid
PG	Prostaglandins
TXA2	Thromboxane A2
LT	Leukotrienes
EET	Epoxyeicosatrienoic acid
DHET	Dihydroxyeicosatrienoic acid
20-HETE	20-hydroxyeicosatetraenoic acid
PPARα	Peroxisome proliferator-activated receptor-α
CCl4	Carbon tetrachloride
NF-κB	Nuclear factor-kappa B
GPR75	G-protein coupled receptor 75
EGFR	Epidermal growth factor receptor
MAPK	Mitogen-activated protein kinase
ACE	Angiotensin-converting-enzyme
TNFα	Tumor necrosis factor alpha
IL-1β	Interleukin 1 beta
IL-6	Interleukin 6
VEGF	Vascular endothelial growth factor

MMP-9	Matrix metalloproteinase-9
PI3K	Phosphoinositide 3-kinase
ERK1/2	Extracellular signal-regulated kinase 1/2
NSCLC	Non-small cell lung cancer
SNP	Single nucleotide polymorphism
NAFLD	Non-alcoholic fatty liver disease
NCBI	National center for biotechnology information
HET0016	N-Hydroxy-N'-(4-butyl-2-methylphenyl)-formamidine
CBC	Complete blood count
mRNA	Messenger RNA
Hb	Hemoglobin
DMSO	Dimethyl sulfoxide
PBS	Phosphate-buffered saline
IP	Intraperitoneally
ICUC	Institutional Animal Care and Use Committee
CHOP	Children's Hospital of Philadelphia
DHE	Dihydroethidium
HPLC	High Performance Liquid Chromatography
HBSS	Hanks' balanced salt solution
DTPA	Diethylenetriaminepentaacetic acid
EOH	2-hydroxyethidium
RLU	Relative light units
PCR	Polymerase Chain Reaction
RIPA	Radioimmunoprecipitation assay
BSA	Bovine serum albumin
H&E	Hematoxylin and Eosin
RGB	Red, green, and blue
4-HNE	4-hydroxynonenal
IHC	Immunohistochemistry
NAS	NAFLD Activity Score
AUB	American University of Beirut
NaOH	Sodium hydroxide
NGS	Normal goat serum
DAB	3,3'-diaminobenzidine
MDA	Malondialdehyde
GSH	Glutathione
ELISA	Enzyme-linked immunosorbent assay
ANOVA	Analysis of Variance
SD	Standard deviation
MCV	Mean cellular volume
RDW	RBCs distribution width
WBC	White blood count
ALT	Alanine transaminase
AST	Aspartate transaminase

GGT	Gamma-glutamyl transferase
ALP	Alkaline phosphatase
TSAT	Transferrin saturation
BUN	Blood urea nitrogen
NTA	Nitrilotriacetic acid
SCD	Sickle cell disease
AKI	Acute kidney injury
ATIIR1	Angiotensin II receptor 1
HFD	High fat diet
ARBs	Angiotensin II receptor blockers

INTRODUCTION

1. The Thalassemias

1.1. Epidemiology, and Molecular and Clinical Forms

The Thalassemias are among the most common inherited monogenic disorders worldwide, characterized by defects in the production of adult hemoglobin (1-3). The epidemiology of various forms of thalassemia remains underrecognized. However, the disease is highly prevalent in regions extending from sub-Saharan Africa through the Mediterranean, the Middle East, the Indian subcontinent, and East and Southeast Asia (4-7). Due to ongoing migration, the thalassemias are now also found in Europe and North America, making this disease a global health concern (8-13).

Developmental hemoglobin synthesis is controlled by two multigene clusters located on chromosome 16 (encoding the α-like globins) and chromosome 11 (encoding the β-like globins) (14) **(Figure 1)**. The genes within these clusters are arranged along the chromosome in the order of their expression during development, producing different hemoglobin tetramers during embryonic, fetal, and adult life. In fetal life, the predominant form of hemoglobin is HbF (α2γ2), which is replaced by adult hemoglobin HbA (α2β2) after birth (3, 15). Defects in the α-globin or β-globin gene clusters at the molecular level result in defective hemoglobin synthesis, leading to various inherited forms of either α-thalassemia or β-thalassemia. The type and severity of these clinical forms can be influenced by additional intrinsic and extrinsic factors (15-17).

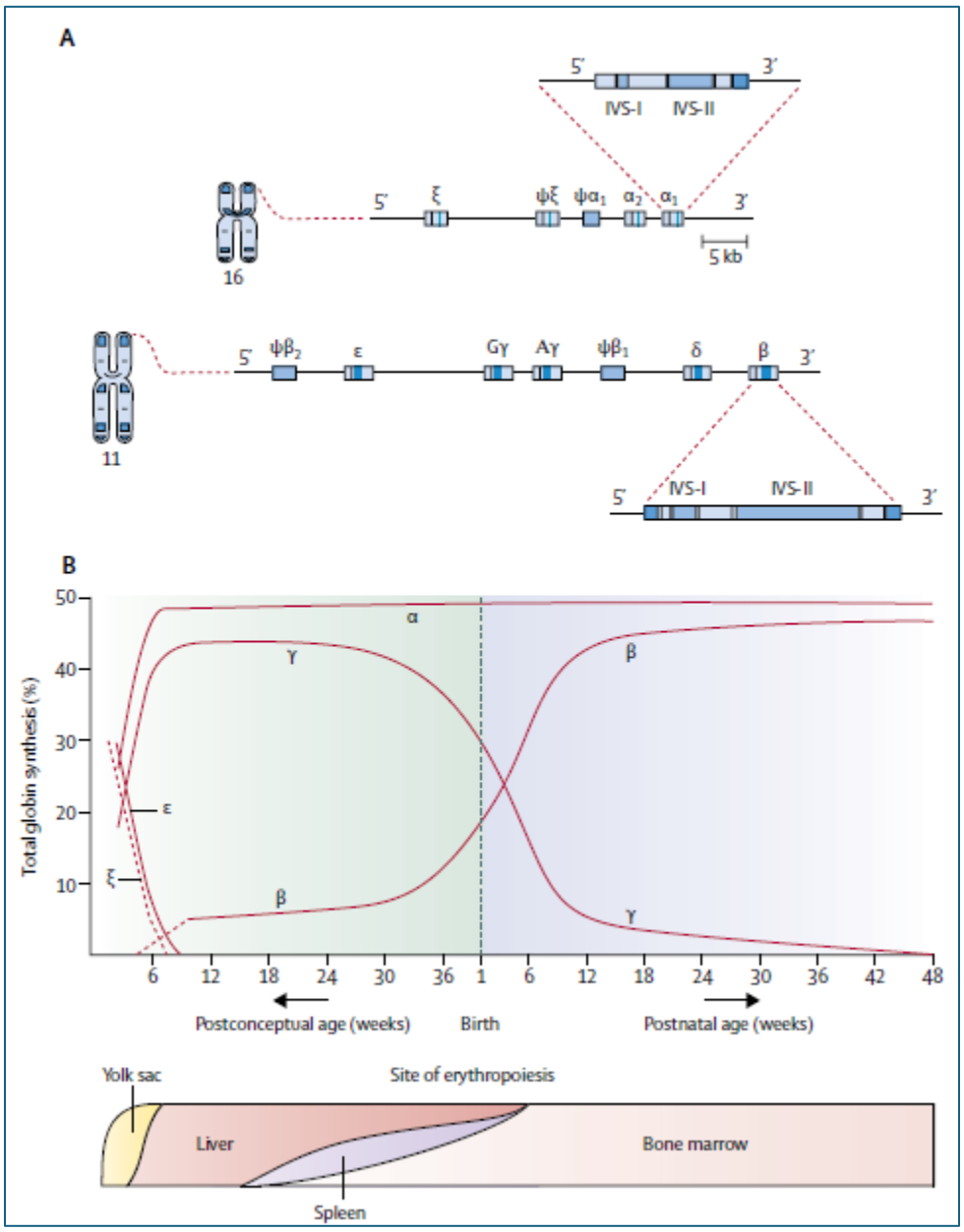

Figure 1. Globin synthesis at the Molecular Level (A) Schematic representation of the organization of the α-globin gene cluster on chromosome 16 and the β-globin gene cluster on chromosome 11. (B) Depiction of the sites of erythropoiesis and the corresponding pattern of globin gene expression throughout developmental stages. Pseudogenes, indicated by ψ, are non-functional and non-expressing. The three exons of each globin gene are highlighted in light blue. Reproduced from Taher AT et al. Lancet. 2018.

Patients with β-thalassemia have traditionally been categorized as minor, major, or intermedia, based on their α-/β-globin chain imbalance, severity of anemia, and clinical presentation. Over the past decade, however, there has been a major shift in the classification of β-thalassemias. The traditional classification, based on molecular forms, has evolved into a system based on clinical management criteria. Since transfusion therapy is the standard and conventional treatment modality for β-thalassemia, the frequency and extent of transfusion requirements indirectly reflect the disease's severity. The use of blood transfusions in these patients can control most of the underlying pathophysiological mechanisms but can also contribute to secondary morbidity (18, 19). Therefore, thalassemia patients are now commonly classified as having transfusion-dependent thalassemia (TDT) or non-transfusion-dependent thalassemia (NTDT). Patients with TDT commonly present with severe anemia in their early childhood that requires lifelong blood transfusions for survival (19). Patients with TDT typically present with severe anemia in early childhood, necessitating lifelong blood transfusions for survival (19). In contrast, NTDT patients usually present with mild-to-moderate anemia later in childhood or adulthood and only require occasional transfusions in specific clinical situations to prevent or manage certain disease complications (20, 21) (**Figure 2**).

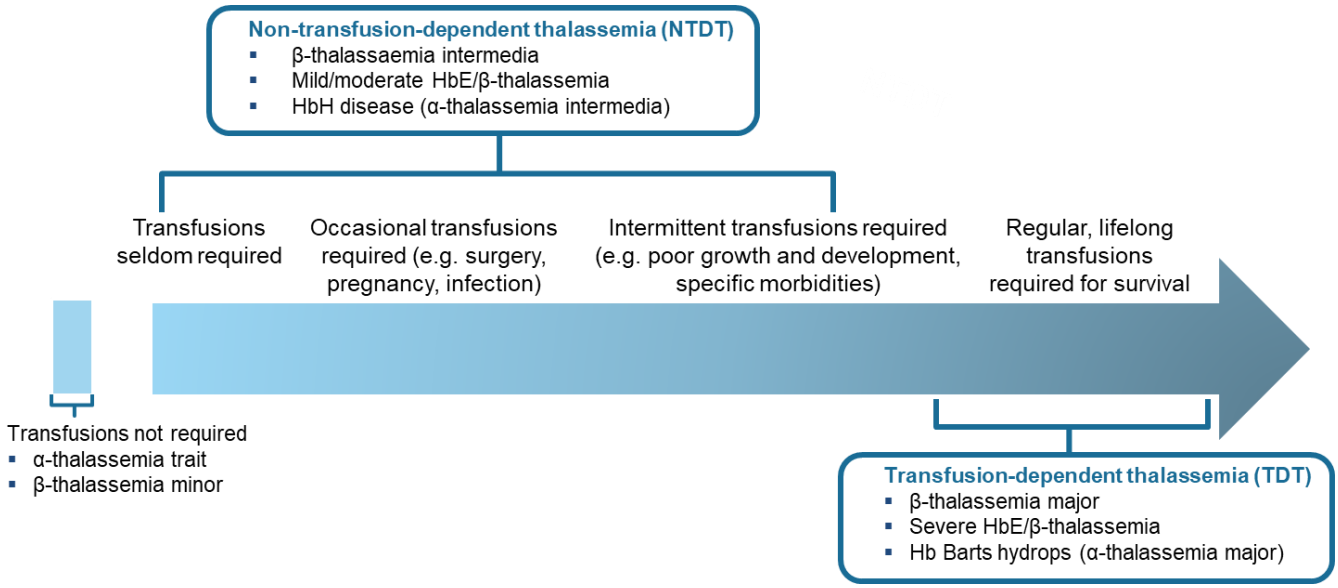

Figure 2. Clinical Classification of Thalassemia based on Transfusion requirement.

Modified from Musallam KM et al. Haematologica 2013.

1.2. Pathophysiology and Associated Morbidity in β-Thalassemia

Clinical complications in β-thalassemia are primarily related to the underlying pathophysiological mechanisms, including ineffective erythropoiesis, chronic hemolytic anemia, and iron overload **(Figure 3)**.

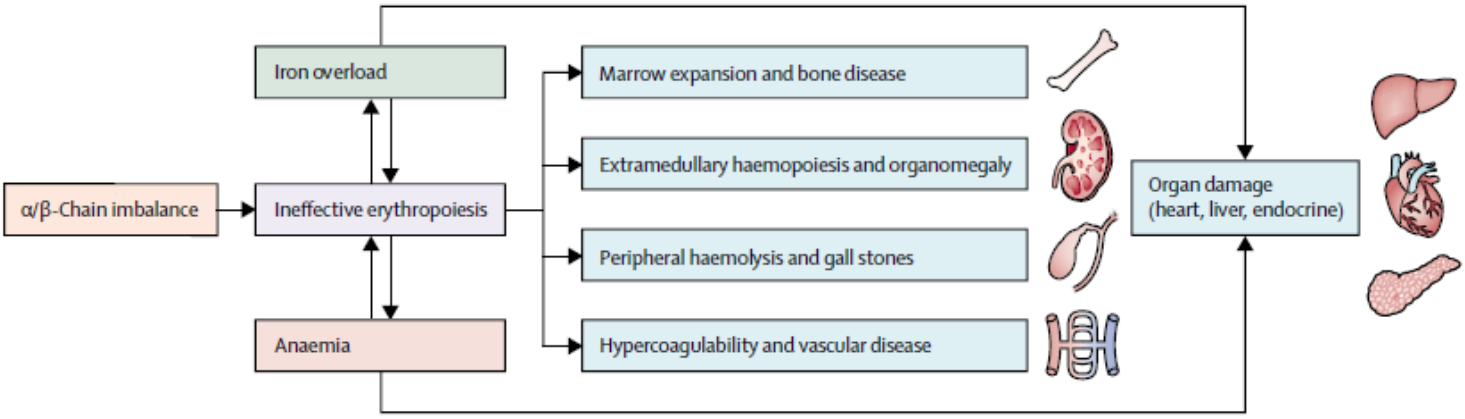

Figure 3. Pathophysiology of Patients with Thalassaemia Syndromes.

Reproduced from Taher AT et al. Lancet. 2018.

Given that regular red blood cell (RBC) transfusion therapy is vital to the disease profile of patients with TDT, many of the pathogenic mechanisms and associated complications are more frequently observed in patients with NTDT. In contrast, adverse effects related to RBC transfusions, such as secondary iron overload and subsequent organ dysfunction, are well-known contributors to the clinical morbidity profile in well-transfused TDT patients (22-25) **(Figure 4)**.

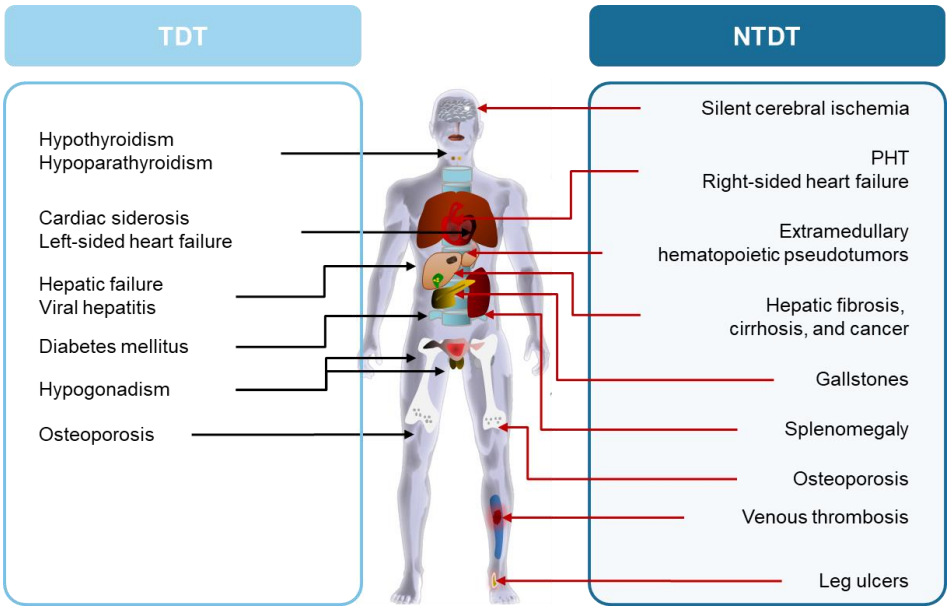

Figure 4. Comparative Overview of Complications and Morbidity Profile in TDT vs. NTDT.
Reproduced from Taher AT et al. Blood Cells Mol Dis 2006.

1.2.1. Iron Overload in β-Thalassemia

Iron overload is of clinical concern in patients with β-thalassemia and can cause substantial morbidity and mortality (26, 27). Traditionally, iron burden has been assessed by measuring serum ferritin levels; however, advancements in magnetic resonance imaging (MRI) have now enabled the precise quantification of iron concentration in a noninvasive manner in target organs, allowing for more personalized management.

The mechanism of iron overload development differs between TDT and NTDT patients. In TDT patients, iron overload development is secondary to red blood cell transfusion. This accumulation of iron in organ tissues can become apparent in children with TDT as young as 2 to 6 years old, and over time, the cumulative iron burden can lead to toxicity and dysfunction in various organs, such as the heart, liver, and endocrine glands (19, 28, 29). In NTDT, ineffective erythropoiesis and hypoxia lead to a reduction in the production of the hepatic hormone hepcidin, resulting in increased intestinal iron absorption and enhanced iron release from macrophages in the reticuloendothelial system. Erythroferrone (ERFE), a hormone secreted by erythroblasts in response to the activation of the erythropoietin receptor–Janus kinase 2–signal transducer and activator of transcription 5 (EPOR–JAK2–STAT5) pathway, serves as the primary erythroid regulator of this process. Other erythroid regulators of hepcidin have been proposed, including growth differentiation factor 15 (GDF15) and twisted gastrulation 1 (TWSG1) (30). In NTDT patients, iron overload gradually increases with age, and concerns about secondary morbidities typically arise after the age of 10 to 15 years (31, 32).

1.2.2. Liver Disease in β-Thalassemia

For the purpose of this project, we will discuss and highlight the pathogenesis of liver disease in β-thalassemia. Liver disease is emerging as a significant cause of mortality in patients with TDT, particularly as advancements in cardiac iron monitoring and effective iron chelation therapy strategies have significantly reduced deaths from heart failure (33). This shift in mortality patterns highlights the growing importance of managing hepatic complications in these patients. Additionally, liver disease accounts for at least 10% of deaths in patients with NTDT,

underscoring its critical role in the overall morbidity and mortality associated with β-thalassemia, regardless of transfusion status (34).

In patients with β-thalassemia, liver disease is primarily driven by iron overload and viral hepatitis, which together contribute to chronic inflammation, fibrosis, and cirrhosis, ultimately increasing the risk of hepatocellular carcinoma (HCC) (35). In cases of hepatic iron overload, free iron or NTBI play a critical role in mediating damage to both hepatic and extra-hepatic tissues (36). The accumulation of iron in the liver, particularly within hepatocytes and other liver cells, triggers a severe state of oxidative stress and leads to the overproduction of reactive oxygen species (ROS). This oxidative stress results in lipid peroxidation and protein damage, contributing to hepatic inflammation and cell necrosis. Over time, these processes drive the development of fibrosis, which can progress to cirrhosis and ultimately lead to HCC (37).

Chronic infection with hepatitis B virus (HBV) or hepatitis C virus (HCV), when coupled with the hepatotoxic effects of iron overload, significantly elevates the risk of accelerated liver fibrosis in patients with β-thalassemia (38). The synergistic impact of persistent viral infection and excessive iron deposition exacerbates liver damage, leading to a more rapid progression of fibrosis. This combination presents a major challenge in managing liver health in β-thalassemia patients, as both factors contribute to the worsening of liver function and increase the likelihood of severe hepatic complications.

Additional factors such as obesity and alcohol consumption can exacerbate liver complications in patients with β-thalassemia. These factors contribute to increased steatosis and oxidative stress, which, in turn, accelerates hepatic iron accumulation. This cascade of events significantly raises the risk of liver fibrosis, cirrhosis, and HCC in these patients (39). The

interplay between these lifestyle factors and iron toxicity underscores the importance of comprehensive management strategies to mitigate liver disease progression in β-thalassemia.

1.3. Oxidative Stress in β-Thalassemia

Although oxidative stress is not the primary etiology of β-thalassemia, it mediates several of its pathologies (40, 41). The main causes of oxidative stress in β-thalassemia are the degradation of the unstable hemoglobin and iron overload (42). Both of these factors lead to the production of free radicals that exceed the cell's antioxidant defenses, resulting in cellular damage and organ dysfunction. Additionally, studies have shown that oxidative stress can be exacerbated by ineffective erythropoiesis and anemia. Among the symptoms aggravated by oxidative stress are increased intravascular and extravascular hemolysis, and dysfunction of critical organs such as the heart, liver, and endocrine system.

1.3.1. Oxidative Stress and Hemoglobin Instability

β-thalassemia is characterized by an unbalanced production of globin chains, leading to an excess of free α-globins (43). These unstable α-globins are prone to auto-oxidation, denaturation, and subsequent precipitation as hemichromes (44, 45). Hemichromes then attach to the cytoplasmic domain of band 3, facilitating oxidative cross-linking through disulfide bonds. This process results in the release of both heme and free iron, causing globin proteins to precipitate. This initiates a self-amplifying redox reaction that further oxidizes hemoglobin molecules, depletes the cell's reducing potential, and triggers phosphorylation responses. These events ultimately destabilize the red blood cell membrane and accelerate the removal of RBCs by splenic macrophages (43, 46, 47).

1.3.2. Oxidative Stress and Ineffective Erythropoiesis

Ineffective erythropoiesis is a key pathophysiological factor in β-thalassemia. The imbalance between α and β globin subunits leads to the accumulation of unbound α-chains during erythroblast maturation. These α-chains tend to bind to heme, eventually forming hemichromes that precipitate and attach to the plasma membrane. (48, 49). Oxidative stress resulting from ineffective erythropoiesis is supported by studies on bone marrow and developing erythroid precursor cells in thalassemia. Research on the bone marrow of β-thalassemia patients has revealed an increased number of activated macrophages, likely responding to the presence of numerous damaged erythroblasts (50, 51). Additionally, oxidative stress induces the expression of growth differentiation factor 11 (GDF11), a ligand of the transforming growth factor β (TGF-β) superfamily, suggesting the existence of an autocrine amplification loop that exacerbates ineffective erythropoiesis. (52). In developing thalassemia erythroid precursors, oxidative stress has been linked to increased apoptosis, as indicated by the externalization of phosphatidylserine (PS). This observation suggests that oxidative stress not only results from ineffective erythropoiesis but may also contribute to it (53).

1.3.3. Oxidative Stress and Anemia

Chronic anemia in β-thalassemia can lead to tissue hypoxia, which in turn can induce the overproduction of ROS. Hypoxia-inducible factor (HIF)-1, a transcriptional activator with an oxygen-regulated subunit, plays a critical role in the cell's adaptive response to prolonged hypoxia. HIF-1 mitigates ROS production under low oxygen conditions through several mechanisms. These include a subunit switch in cytochrome c oxidase, replacing COX4-1 with the more efficient COX4-2 subunit in complex IV; the induction of pyruvate dehydrogenase kinase 1 (PDK1), which redirects pyruvate away from the mitochondria; the activation of BNIP3,

which initiates selective autophagy of mitochondria; and the upregulation of microRNA-210, which inhibits the assembly of iron-sulfur (Fe/S) clusters necessary for oxidative phosphorylation (54).

1.3.4. Oxidative Stress and Iron Overload

Iron overload is another significant contributor to oxidative stress in β-thalassemia (55). Under normal conditions, iron in the plasma is bound to transferrin for safe transport. However, in patients with β-thalassemia, iron overload overwhelms the transferrin system, leading to the production of non-transferrin-bound iron (NTBI) and labile plasma iron (LPI). Both NTBI and LPI circulate freely in the plasma and eventually accumulate within susceptible cells. (56, 57). Over time, the continuous uptake of NTBI and LPI results in increased levels of storage iron and labile cellular iron (58). When the accumulation of this labile iron exceeds the cell's capacity to synthesize new ferritin, a critical concentration is reached. This intracellular labile iron is redox-active and can catalyze the Fenton and Haber-Weiss reactions, leading to the generation of ROS (59). The excessive production of ROS due to iron overload, particularly from NTBI, plays a crucial role in inducing cellular dysfunction, apoptosis, and ferroptosis in β-thalassemia. (60-63).

2. Evolutionary Perspective of a Redox Balance and Intracellular Sources of ROS

Reactive oxygen species are chemically reactive molecules generated as by-products of various cellular metabolic processes. These include hydrogen peroxide (H2O2), superoxide radicals (O2•−), and nitrogen-based species like peroxynitrite (ONOO−) and nitric oxide (NO) (64, 65). They are important cellular entities involved in processes such as cell proliferation, signal transduction, immune defense, homeostasis, and gene regulation (66).

Reactive oxygen species have evolved alongside natural and environmental changes, serving as heritable biological adaptations. Understanding these evolutionary adaptations has provided crucial insights into the roles and mechanisms of ROS. A key aspect of physiological function is that cellular activities are regulated by fixed and coordinated set points, a phenomenon known as homeostasis (67). Levels of ROS are tightly controlled by cellular antioxidants to maintain a redox balance. All cells possess effective antioxidant systems that neutralize and eliminate ROS, and several enzymatic pathways in the body can convert ROS into less harmful substances (68).

Reactive oxygen species function as specific mediators and second messengers in cell signaling, and can affect vascular tone, immune responses, cellular protection, and hormone actions (69-71). These roles are maintained through a balance between ROS and antioxidative mechanisms that regulate the bioavailability of oxidative species. However, in pathological conditions, an excess of oxidant radicals can lead to oxidative stress, disrupting cellular homeostasis and causing damage to organelles, particularly cellular membranes, potentially leading to cytotoxicity and organ failure (40).

Numerous studies have shown that elevated ROS levels are directly linked to irreversible oxidation of cellular components, contributing to cell dysfunction and necrosis (72). However, reducing ROS levels too drastically can be harmful, as low concentrations of ROS are essential for signaling (73). This underscores the importance of the redox system in cellular physiology and the need to maintain a delicate balance between oxidant and antioxidant molecules (74). Current research is focused on identifying specific sources of ROS production that are altered in a cell- and disease-specific manner.

All types of cells can generate ROS through various mechanisms. These include non-enzymatic processes, such as those occurring in the mitochondrial electron transport chain, as well as enzymatic reactions involving Nicotinamide adenine dinucleotide phosphate (NADPH) oxidases and cytochrome P450 (CYP450). Each of these sources plays distinct physiological roles and contributes differently to organ function and related diseases (75-77). Additional intracellular ROS sources include the mitochondria, xanthine oxidase, uncoupled nitric oxide synthase (NOS), cyclooxygenases (COX), and lipoxygenases (LIPOX) (78) **(Figure 5)**. When ROS production exceeds the cellular antioxidant defenses, it leads to cellular damage, in the form of disrupted metabolism, oxidation of proteins and lipids, activation of transport and signaling pathways, and ultimately, apoptosis (79).

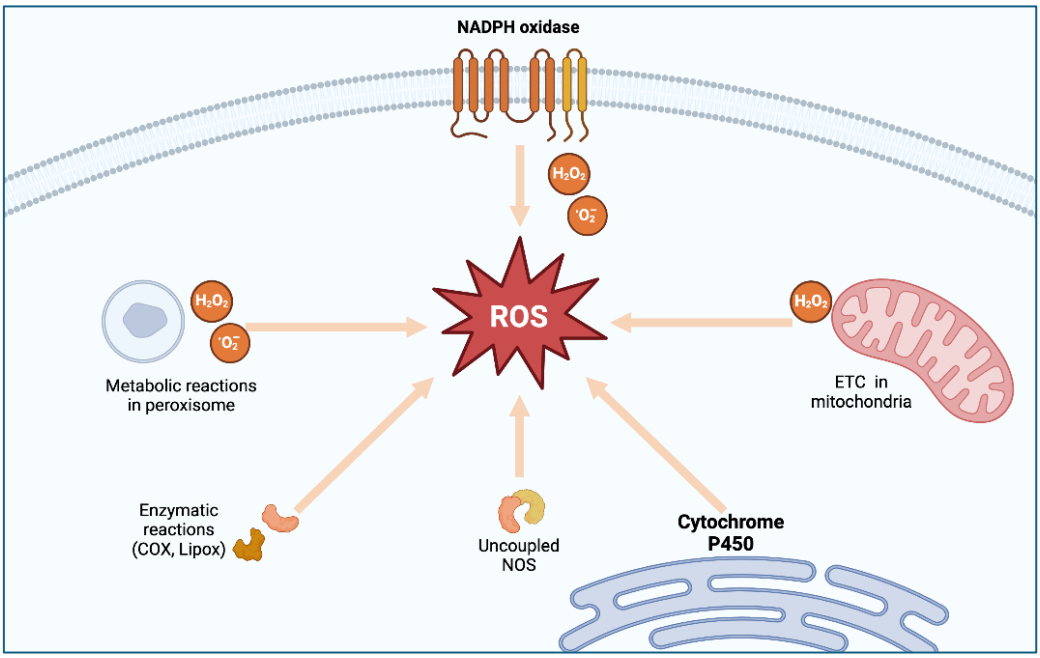

Figure 5. Intracellular Sources of ROS

3. Metabolism Pathways of Arachidonic Acid

The omega-6 polyunsaturated fatty acid (PUFA), or arachidonic acid (AA), and its metabolites have garnered significant interest in recent years due to their roles and involvement in inflammatory processes and disease (80). The biological significance of AA stems from its metabolism by three distinct enzyme systems: COXs, LOXs, and CYP450 enzymes (**Figure 6**). These systems produce a diverse array of biologically active fatty acid mediators.

Cyclooxygenases are the enzymes responsible for metabolizing AA into prostanoids, which include prostaglandins (PGs) and thromboxane A2 (TXA2). The process begins with the release of AA from the plasma membrane by phospholipases, followed by its conversion into PGG2 and PGH2 by COX enzymes. These intermediates are then further processed into PGs by specific PG synthases. There are two main COX isoforms: COX-1, which is constitutively expressed in most cells and primarily produces prostanoids involved in routine physiological functions; and COX-2, which is induced by inflammatory stimuli, hormones, and growth factors, and is generally regarded as the major source of prostanoids during inflammation and in conditions such as cancer. The LOX pathway was the second eicosanoid and inflammatory pathway to be targeted for therapeutic intervention. Enzymes within this pathway produce leukotrienes (LTs). The third pathway for metabolizing AA is the CYP450 pathway. While the CYP enzyme family comprises various subclasses, ω-hydroxylase and epoxygenase activities are particularly significant for AA metabolism (80).

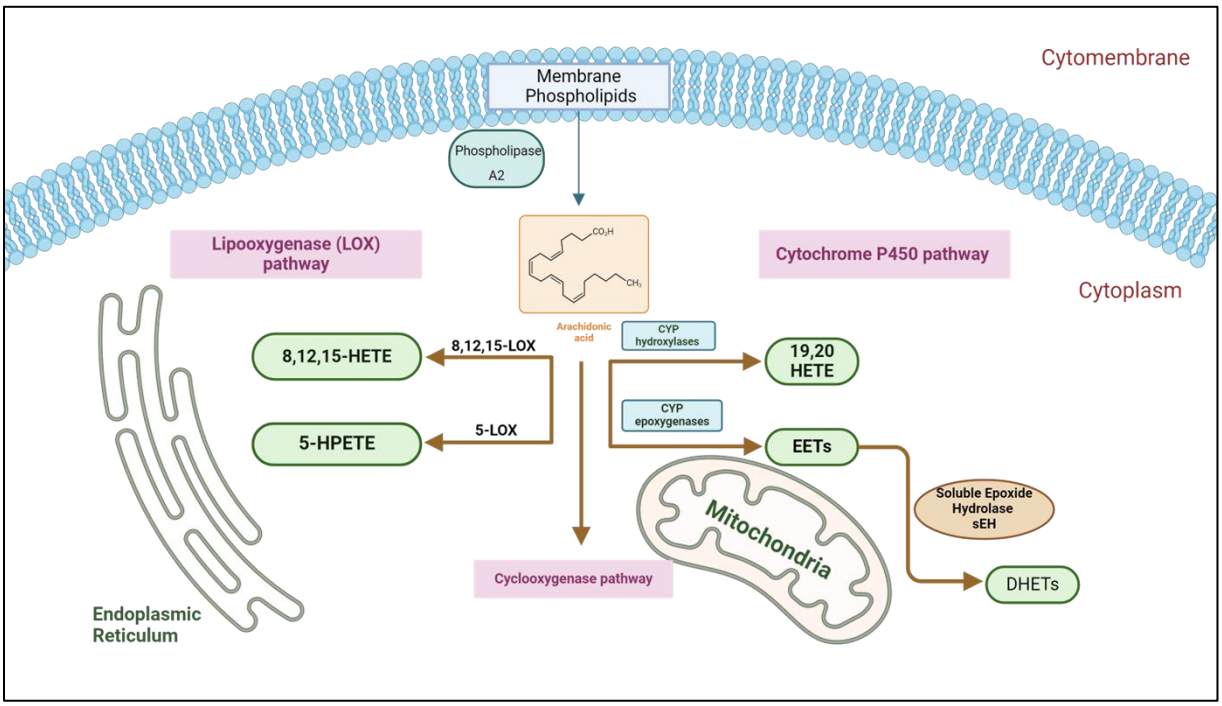

Figure 6. Overview of the AA Metabolism Pathways. Phospholipase enzymes, such as PLA2, are responsible for releasing free AA from phospholipid membrane. The COXs metabolize AA to protanoids, prostacyclin, and thromboxane. The LOXs metabolize AA to leukotrienes and HETEs. The P450 epoxygenases metabolize AA to midchain HETEs and EETs. All EETs are then further metabolized to less active DHETs by sEH.

4. A closer Look at Cytochrome P450 Pathway

CYP450 enzymes are a large family of hemoproteins involved mediating the oxidation reactions of many endogenous and exogenous compounds in the human body. These enzymes are located in the membranes of mitochondria or the endoplasmic reticulum and are known for their role in redox reactions (81). Additionally, CYP450 is a significant source of species ROS in various tissues, impacting a wide range of disease conditions. (82-86).

In the CYP450-catalyzed monooxygenase pathway, the major products include regiospecific and stereospecific epoxyeicosatrienoic acids (EETs), their corresponding dihydroxyeicosatrienoic acids (DHETs), and 20-hydroxyeicosatetraenoic acid (20-HETE)

(Figure 7). (87, 88). These eicosanoids, derived from CYP450 activity, are produced in a cell- and tissue-specific manner and have diverse biological functions. They act as second messengers, regulating vascular tone and ion transport (89, 90), and have recently been implicated in critical processes such as cellular proliferation, inflammation, and hemostasis (88, 91).

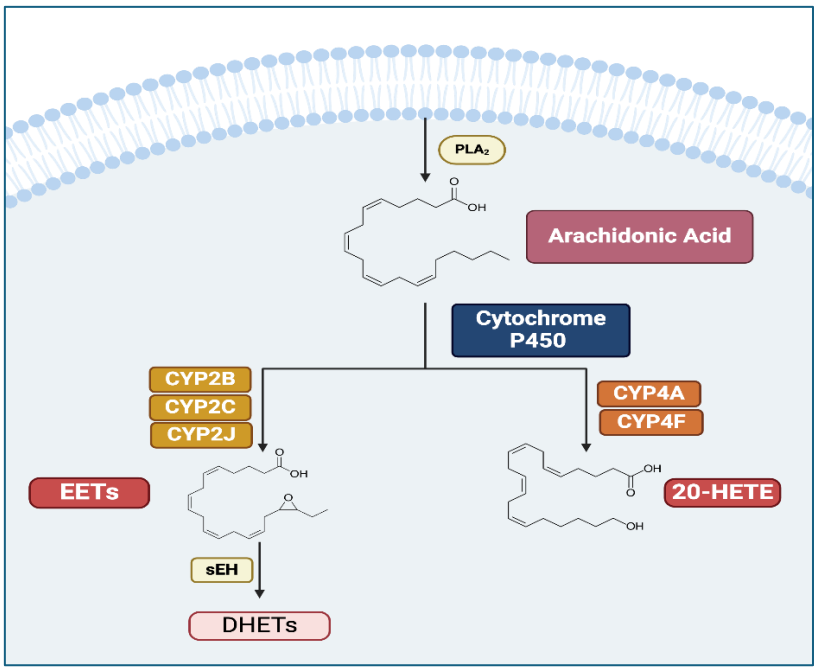

Figure 7. Summary of the CYP450-catalyzed Monooxygenase Pathway. Free AA is metabolized via the CYP450 enzymes, CYP2B, CYP2C and CYP2J (which belong to the epoxigenase family) to produce EETs and by CYP4A or CYP4F enzymes (which belong to the hydroxylase family) to produce 20-HETE.

4.1.Classification and Tissue Distribution of the CYP4 Family in Humans

For this project, we will focus on the ω-hydroxylation of AA, which generates 20-HETE and is catalyzed by the CYP4A family of enzymes (88, 89, 92). Although there are more than 11 subfamilies of CYP4 in different species, only 6 subfamilies of CYP4 genes have been reported in humans. The human CYP4 subfamilies are CYP4A, CYP4B, CYP4F, CYP4V, CYP4X, and CYP4Z (93). While ω-hydroxylation by CYP4A occurs in various organs, it is particularly

prominent in the kidney and liver, where it is associated with significant physiological functions (88, 94-97). In humans, two highly homologous CYP4A genes, CYP4A11 and CYP4A22, are located on chromosome 1 (98, 99). Moreover, research has shown that CYP4A11 accounts for approximately 13% to 33% of 20-HETE production through the ω-hydroxylation of AA in the liver and kidney (97). The precise functions of CYP4A22, however, remain largely unexplored.

Members of the CYP4F subfamily are also known to catalyze ω/ω-1 hydroxylation of arachidonic acid, with a predominant role in the kidney (97, 100). This subfamily includes seven CYP4F isoforms (CYP4F2, CYP4F3A, CYP4F3B, CYP4F8, CYP4F11, CYP4F12, and CYP4F22) encoded by six distinct genes located in the CYP4F gene cluster on chromosome 19. Among these, CYP4F2 is the most extensively studied. It has been reported to be predominantly found in various tissues and organs, including the liver, kidney, lung, white blood cells, and notably in the endoplasmic reticulum (101, 102).

4.2. Classification and Tissue Distribution of the CYP4 Family in Mice

The mouse Cyp4a subfamily mainly includes Cyp4a10, Cyp4a1a, Cyp4a12b, and Cyp4a14. These are mostly expressed in organs such as the kidney and liver. In mice, the expression levels of Cyp4a mRNA in the liver and kidney are also influenced by sex hormones and growth hormones (103). Because of this, there are notable gender differences in the expression of CYP ω-hydroxylases. Specifically, Cyp4a10 is expressed in both male and female mice, while Cyp4a12a is expressed exclusively in males and is regulated by androgens. Cyp4a14, on the other hand, shows a strong expression pattern in female mice (104). The mouse Cyp4f subfamily includes Cyp4f13, Cyp4f14, Cyp4f15, Cyp4f16, Cyp4f17, Cyp4f18, Cyp4f37, and

Cyp4f39, with expressions across various tissues, mainly liver and kidney. **Table 1** summarizes the different isoforms of the CYP4A and CYP4F expressed in humans and the equivalent expressed in mouse, in addition to the organs where they are expressed.

Table 1. CYP ω-hydroxylase orthologous genes expressed in various mouse and human organs.

Human	Organs	Cell Type Specificity	Mouse	Organs
4A11	liver, kidney, small intestine, lung, heart, skin, adrenal, prostate, testis, uterus, mammary, placenta	hepatocytes, proximal tubular cells	*4a10*	liver, kidney
4A22	liver, kidney	hepatocytes	*4a12a*	liver, kidney
			4a12b	liver, kidney, lung
			4a14	liver, kidney
			4a29	testis, thymus
			4a30b	colon, testis
			4a31	kidney, liver
			4a32	kidney, liver
4F2	liver, small intestine, kidney, brain, skin, prostate, testis	hepatocytes	*4f13*	liver, kidney, lung, heart, testis
4F3	liver, small intestine, trachea, kidney, prostate	hepatocytes	*4f14*	liver, kidney, brain, testis
4F8	small intestine, lung, stomach, kidney, skin, eye, adrenal, prostate, urinary bladder, testis, uterus	urothelial cells, glandular cells, granulocytes	*4f15*	liver, kidney, lung, brain
4F11	liver, colon, heart, brain, skeletal muscle, ovary, placenta, kidney	hepatocytes, ductal cells, urothelial cells	*4f16*	liver, kidney, lung, brain, heart, spleen
4F12	liver, small intestine, stomach, colon, kidney, heart, skin, prostate, ovary, placenta	enterocytes, Paneth cells, undifferentiated cells	*4f17*	ubiquitous expression in subcutaneous fat pad adult, ovary and 26 other tissues
4F22	liver, small intestine, kidney, brain, skin, skeletal muscle, testis, placenta	granulocytes, Suprabasal keratinocytes, glandular cells, spermatogonia	*4f18*	liver, kidney, lung, spleen, ovary
			4f37	duodenum, large intestine and 20 other tissues
			4f39	stomach, testis, bladder, kidney, lung
			4f40	testis, colon, duodenum

5. Role of 20-HETE in Health and Disease

5.1. Role of 20-HETE in the Liver

Numerous functional roles for 20-HETE have been reported in the liver. Some studies have shown that 20-HETE participates in the regulation of liver metabolic activity and hemodynamics (105, 106). Moreover, 20-HETE is a powerful activator of peroxisome proliferator-activated receptor-α (PPARα), playing a critical role in lipid homeostasis and the regulation of fat-dependent energy supply and metabolism (107, 108). Additionally, it functions as a significant inflammatory mediator and may have a substantial impact on inflammatory diseases.

However, 20-HETE has also been implicated in various disease pathologies, including liver disorders such as fibrosis, and cirrhosis (105, 109, 110). For example, data from studies conducted on patients with hepatic cirrhosis showed that 20-HETE production was increased in the pre-glomerular microcirculation zone, and led to the constriction of renal vasculature, reduction of renal blood flow and decrease in renal hemodynamics (105, 109). Another study also showed that 20-HETE was significantly increased in mice with carbon tetrachloride (CCl4)-induced liver fibrosis (110). These results suggest that 20-HETE plays an important role in the pathogenesis of hepatic fibrosis and may be a possible target for the clinical treatment of hepatic fibrosis.

5.2. Role of 20-HETE in Inflammation

Vascular inflammation plays a critical role in the development of various diseases, including atherosclerosis, hypertension, and vascular remodeling. CYP ω-hydroxylase and 20-

HETE have been reported to play an important role in vascular inflammation. This is significant for a disease like β-thalassemia, which is characterized by an increase in endothelial cell activation, vascular inflammation, and hypercoagulability (111, 112).

20-HETE has been shown to contribute to vascular inflammation by increasing the expression of adhesion molecules and inflammatory cytokines through endothelial cell activation (113). One study showed that 20-HETE can activate nuclear factor-kappa B (NF-κB) and stimulate the production of inflammatory cytokines in human endothelial cells (114). Recent research has also demonstrated that 20-HETE binds to the G-protein coupled receptor 75 (GPR75), leading to c-Src-mediated activation of the epidermal growth factor receptor (EGFR) and triggering the downstream mitogen-activated protein kinase (MAPK) pathway. This cascade induces angiotensin-converting enzyme (ACE) expression and causes endothelial dysfunction (115, 116). Additionally, in endothelial cells, 20-HETE has been shown to promote the production of ROS via NADPH oxidase, which subsequently activates the L-type Ca2+ channel (86, 117). In the context of ischemia-reperfusion injury, inhibition of 20-HETE synthesis has been shown to reduce oxidative stress and decrease the expression of vascular tumor necrosis factor alpha (TNFα), interleukin 1 beta (IL-1β), and interleukin 6 (IL-6) (118, 119). Finally, 20-HETE has been shown to be involved in promoting tumor angiogenesis and metastasis by upregulating vascular endothelial growth factor (VEGF) and matrix metalloproteinase-9 (MMP-9) through phosphoinositide 3-kinase (PI3K) and extracellular signal-regulated kinase 1/2 (ERK1/2) signaling pathways in human non-small cell lung cancer (NSCLC) cells (120). **Figure 8** represents a schematic of all signaling cascades involving 20-HETE in inflammatory diseases.

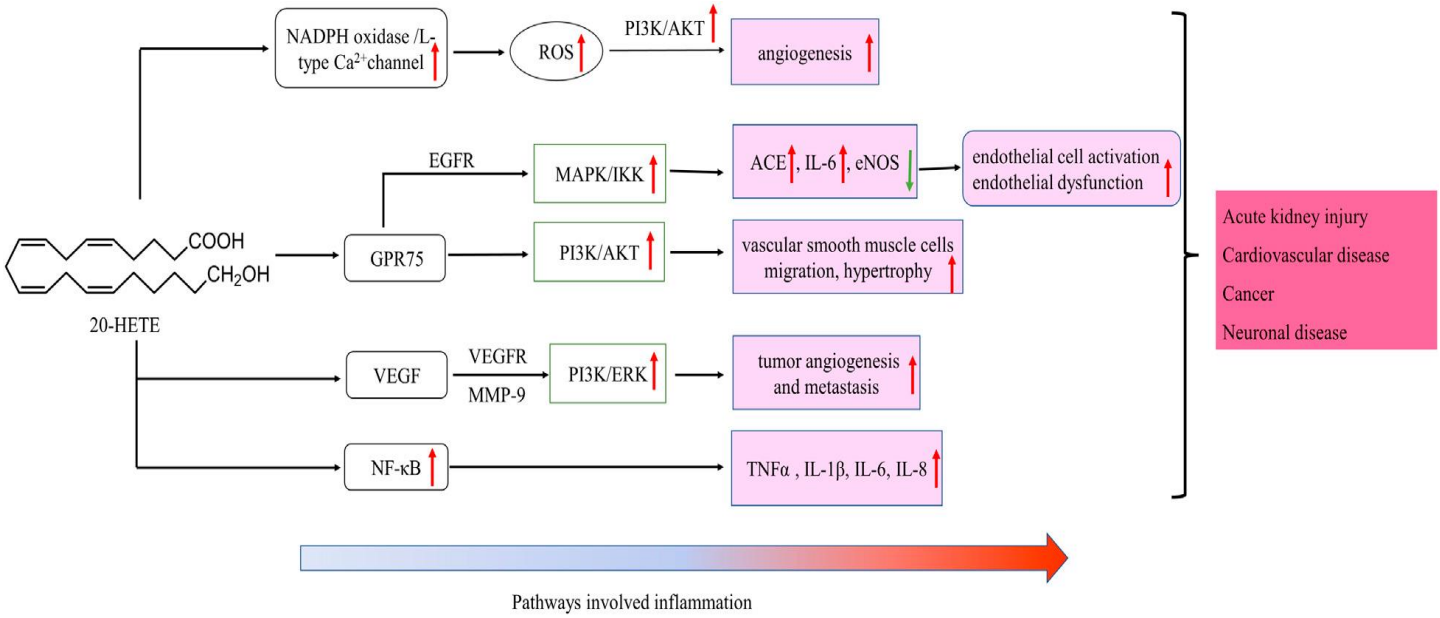

Figure 8. **Schematic Representation of Signaling Pathways involving 20-HETE in Inflammatory Diseases.** ↑: up-regulation; ↓: down-regulation. IL, interleukin; LOX, MAPK/ERK, the mitogen-activated protein kinase/extracellular signal-regulated kinase; NF-κB, nuclear factor-kappa B; TNF-α, tumor necrosis factor alpha; EGFR, epidermal growth factor receptor, VEGF, vascular endothelial growth factor; ROS, reactive oxygen species; PI3K, phosphoinositide 3-Kinases. Reproduced from KD Ni et al. Front Pharmacol. 2021

6. Significance of Single Nucleotide Polymorphisms in Health and Disease

Single nucleotide polymorphisms (SNPs) represent the most basic form of genetic variation, occurring when a single nucleotide is replaced by another. As the most common type of genetic polymorphism in the human genome, SNPs are increasingly being studied due to their significant impact on disease susceptibility, treatment responses, and overall health (121). They are particularly relevant in the context of genetic predisposition to liver diseases, such as HCC, non-alcoholic fatty liver disease (NAFLD) (122, 123). SNPs can be found in both coding and noncoding regions of DNA. When present in coding regions, they may be silent (synonymous) or may change the amino acids encoded by the gene (non-synonymous). Notably, SNPs across the genome have been linked to variations in DNA methylation levels—a key epigenetic

modification that regulates gene expression without altering the DNA sequence itself. SNPs can affect these methylation patterns, influencing gene activity and potentially contributing to disease development and progression (124-126). Given their abundance and stability, SNPs are valuable for identifying individuals at risk, predicting disease outcomes, and more importantly, assessing treatment responses, making them promising candidates for genetic biomarkers.

7. Molecular Functionality of CYP450 Genetic Polymorphisms

Numerous studies have reported associations between SNPs and the development of liver diseases. Given that 20-HETE is implicated in liver disease abnormalities, it is important to investigate how genetic variants in CYP4 genes can contribute to individual differences in metabolism and disease susceptibility. Understanding these genetic variations can provide insights into how these SNPs can potentially influence the degree of 20-HETE production (127) .

7.1. Genetic Variants of CYP4A11, CYP4A22 and CYP4F2

Genetic variants in the CYP4A11 and CYP4F2 genes have been linked to cardiovascular conditions such as hypertension (128-130). The national center for biotechnology information (NCBI) database currently lists over 3,400 SNPs for CYP4A11 and approximately 5,900 SNPs for CYP4F2. However, only a subset of these SNPs has demonstrated significant clinical associations with functional changes. Among the well-studied SNPs for CYP4A11 is rs1126742, which results in an amino acid substitution from phenylalanine to serine at position 434. This variant is associated with reduced synthesis of 20-HETE from arachidonic acid (131, 132). Additionally, the CYP4A11 rs9333025 variant has been associated with hypertension and stroke (133). For CYP4F2, the rs2108622 variant is a non-synonymous change that alters the amino acid sequence from valine to methionine, leading to decreased enzymatic activity related to vitamin K

metabolism. Another notable SNP in CYP4F2, rs3093135, has been linked to an increased risk of stroke in addition to blood pressure (133, 134). Research on CYP4A22 polymorphisms has been limited to specific populations, such as Japanese and French populations (135, 136). Moreover, the role of CYP4A22 variants in human diseases remains largely unexplored, due to the gene's low expression levels.

AIMS

Reactive oxygen species are one of the main contributors to pathological outcomes in β-thalassemia, with their generation being a consequence of iron overload and abnormal red blood cell metabolism. We have previously shown that CYP450 mediates ROS production in a mouse model of β-thalassemia through an increase in 20-HETE activity (137). In this study, we assessed the efficacy of N-Hydroxy-N'-(4-butyl-2-methylphenyl)-formamidine (HET0016), an inhibitor of 20-HETE formation, in reducing 20-HETE-mediated oxidative stress and liver injury in mice affected by β-thalassemia. We specifically aimed at:

1. Evaluating the impact of HET0016 on complete blood count (CBC) parameters and body-to-organ weight ratios.
2. Assessing the efficacy of HET0016 in reducing CYP4A messenger RNA (mRNA) and protein expression levels, as well as 20-HETE levels.
3. Evaluating the efficacy of HET0016 in decreasing 20-HETE-induced oxidative stress and lipid peroxidation.
4. Examining the potential of HET0016 to reduce various markers of liver injury, fibrosis, and cell death by using various molecular, histological and biochemical assessments.

Additionally, and in order to translate our in vivo findings to humans, we conducted an observational study on a cohort of β-thalassemia patients to measure and report 20-HETE levels in plasma. We specifically aimed at:

1. Comparing plasma 20-HETE levels in β-thalassemia patients with those in a cohort of healthy individuals, establishing baseline differences.
2. Correlating 20-HETE levels with various clinical parameters in β-thalassemia patients, focusing particularly on markers related to iron metabolism and oxidative stress.

Finally, and to further understand and explore the genetic factors that could influence 20-HETE production, we aimed at:

1. Investigating the impact (if any) of specific functional SNPs in the CYP4A and CYP4F genes on 20-HETE levels within our cohort of β-thalassemia patients.

MATERIALS AND METHODS

1. Animal Study

1.1.Animal Model and Study Design

All animals (C57BL/6 background) were bred at the Children's Hospital of Philadelphia, PA, USA. We used both male and female $Hbb^{th3/+}$ mice (The Jackson Laboratory- B6; 129P2-*Hbb-b1*^{tm1Unc} *Hbb-b2*^{tm1Unc}/J). These mice carry a double knock-out of the *Hbb-b1 and Hbb-b2* adult β-globin genes, with a phenotype like that seen in NTDT. They show moderate anemia with hemoglobin (Hb) levels ranging from 6 to 9 g/dL. Thalassemia diagnosis was confirmed through genotyping and measurement of Hb levels. The study design is as follows:

• **Group 1:** Wild-type animals (C57BL/6J background) were treated with a 1:1 solution of dimethyl sulfoxide (DMSO): phosphate-buffered saline (PBS) (n=11).

• **Group 2:** $Hbb^{th3/+}$ animals (C57BL/6J background) were treated with a 1:1 solution of DMSO:PBS (n=14).

• **Group 3:** $Hbb^{th3/+}$ animals (C57BL/6J background) were treated with HET0016 (n=7).

All animal-model experimental protocols used in this study were approved by the Institutional Animal Care and Use Committee (ICUC) of the of the Children's Hospital of Philadelphia (CHOP), under protocol number IAC 21-001173, with the title "Novel Approaches for the Treatment of Disorders Associated with Inflammation, Abnormal Erythropoiesis and Altered Iron Metabolism". All animals were kept in a temperature-controlled room and on a 12/12-dark/light cycle and had standard chow and water access and were treated according to the

approved protocols and procedures of the facility. On the day of sacrifice, all mice were euthanized via cervical dislocation with anesthesia, and blood was collected for analysis and the liver was harvested. The liver was then cut into various sections: some were stored at -80°C for later analysis, while others were fixed in 4% formaldehyde for subsequent histological examination.

1.2. Drug Preparation, Dose and Mode of Administration

The solubility of HET0016 is approximately 20mg/mL in DMSO. This was then diluted with the aqueous buffer PBS. HET0016 has a solubility of approximately 0.5mg/mL in a 1:1 solution of DMSO:PBS. The drug was administered daily, and intraperitoneally (IP) at a dose of 5mg/kg/day for a total duration of 4 weeks. During the treatment phase, all animals were weighed once weekly and closely monitored for any potential drug adverse event or toxicities.

1.3.Hematological parameters

Blood was collected via retro-orbital puncture under isoflurane anesthesia on two occasions: initially at baseline and again at the end of the treatment period. The collected blood samples were subsequently analyzed in the Translational Core Lab at CHOP using the XN-1000V hematology analyzer.

1.4.Detection of intracellular superoxide using HPLC

The measurement of dihydroethidium (DHE)-derived oxidation products, indicating ROS production in liver tissues, was performed using the High Performance Liquid Chromatography (HPLC) method (138, 139). This method is very sensitive and reliable in detecting superoxide anions compared to immunofluorescent DHE staining and other ROS detection methods. In brief,

liver tissues were first washed twice with Hanks' balanced salt solution (HBSS) containing diethylenetriaminepentaacetic acid (DTPA), then homogenized and incubated for 30 min with 50 μM DHE (Sigma-Aldrich) in HBSS–100 μM DTPA. After incubation, tissues were collected in acetonitrile and centrifuged at 12,000 x g for 10 minutes at 4°C, and then dried under vacuum. The samples were subsequently analyzed using HPLC with fluorescence detection. The concentrations of DHE, 2-hydroxyethidium (EOH), and ethidium products were quantified by comparing the integrated peak areas of the obtained chromatograms with those of standard curves for each product, under identical chromatographic conditions. EOH and ethidium were detected by fluorescence with excitation at 510 nm and emission at 595 nm, while DHE was monitored by ultraviolet absorption at 370 nm. The results were expressed as the amount of EOH produced (in nmol) normalized to the amount of DHE consumed (i.e., the initial DHE minus the remaining DHE in the sample, expressed in μmol).

1.5. NADPH Oxidase Activity

NADPH oxidase activity in the liver tissues was also measured (21). Briefly, liver tissues were homogenized in 200 μL of lysis buffer [20 mM KH2PO4 (pH 7.0), 1 mM EGTA, 1 mM phenylmethylsulfonyl fluoride, 10 μg/ml aprotinin, and 0.5 μg/ml leupeptin]. Tissues were then homogenized using a Dounce homogenizer with 100 strokes on ice. Protein concentrations were quantified using Bio-Rad protein assay reagents. For the NADPH oxidase assay, 25μg of the homogenate was added to a reaction mixture containing 50 mM phosphate buffer (pH 7.0), 1 mM EGTA, 150 mM sucrose, 5 μM lucigenin, and 100 μM NADPH. Photon emission, expressed as relative light units (RLU), was measured every 30 seconds for 5 minutes using a luminometer. The readings were corrected by subtracting the buffer blank, which constituted less than 5% of

the total signal. The results were expressed as RLU per minute (min) per milligram (mg) of protein, indicating the level of NADPH activity.

1.6. Real-time Polymerase Chain Reaction (PCR) and Gene Expression Analysis

RNA extraction was performed using the Direct-zol™ RNA Miniprep (Zymo Research) as per instructions of the manufacturer. Briefly, liver tissues were lysed with TRIZOL reagent (Sigma Aldrich, Steinheim, Germany). An equal volume of ethanol (95-100%) was added to the sample lysed in TRIZOL. The solution was mixed thoroughly to ensure complete interaction between the ethanol and the lysate. The mixture was trasnferred into a Zymo-Spin™ IICR Column placed in a Collection Tube. The column was then centrifuged at highest speed to allow RNA binding to the column matrix. After centrifugation, the flow-through was discarded and the column was placed into a new collection tube. 400 µl of RNA Wash Buffer was added to the column and centrifuged. In an RNase-free tube, the DNase I treatment mix was prepared by combining 5 µl of DNase I (6 U/µl) with 75 µl of DNA Digestion Buffer. This mixture directly to the column matrix and the column was left to incubate at room temperature (20-30°C) for 15 minutes to allow for the digestion of any contaminating DNA. After the incubation, 400 µl of Direct-zol™ RNA PreWash to the column and centrifuged and the flow-through was discarded (repeated 2X). Finally, 700 µl of RNA Wash Buffer was added to the column and centrifuged for 1 minute. This step ensures the complete removal of any residual wash buffer. After centrifugation, the column was carefully put into an RNase-free tube. To elute the purified RNA, 50 µl of DNase/RNase-Free Water was added directly onto the column matrix. This was then centrifuged to collect the eluted and pure RNA in an RNase-free tube. 100ng total RNA was either converted to cDNA using the iScript™ cDNA Synthesis Kit (Bio-Rad Laboratories, Inc) as

per protocol and then quantified using RT- PCR Biorad CFX384, or the GoTaq® Probe 1-Step RT-qPCR System (Promega Corporation, USA) and run on the 7500 Real Time PCR System (ThermoFisher Scientific, USA). The following Taqman probes were used for our gene expression analysis: *GAPDH* (Mm99999915_g1, Thermofischer Scientific), *CYP4A10* (Mm01188913_g1, Thermofischer Scientific), *CYP4A14* (Mm00484132_m1, Thermofischer Scientific), *PPARα* (Mm00440939_m1, Thermofischer Scientific), *HGF* (Mm01135184_m1, Thermofischer Scientific), and *GPX4* (Mm00515041_m1, Thermofischer Scientific). mRNA expression was analyzed by real-time RT-PCR using the ΔΔCt method. All reactions were performed in triplicates. Data were normalized to the expression levels of GAPDH (housekeeping gene) and results were expressed as fold change compared to control.

1.7.Western Blot Analysis

Liver tissues were lysed using a radioimmunoprecipitation assay (RIPA) buffer. Homogenates were incubated for two hours on ice and centrifuged at 13,600 rpm for 30 min at 4°C. The supernatant containing the proteins was collected and stored at -20°C. Protein concentration was measured using bovine serum albumin (BSA) protein assay. A volume of 25µl of samples (containing 50 µg of proteins) were first heated and then loaded on the NuPAGE 4-12% gradient Bis-Tris Gel (1.5mm) and western blot was run (Invitrogen by ThermoFischer Scientific). Samples were then transferred to a nitrocellulose membrane (BioRad, Hercules, CA), and the membrane was then blocked with 5% milk for 1 hour. Blots were then incubated overnight at 4°C with mouse monoclonal anti-CYP4A (1:1000, sc-271983, Santa Cruz Biotechnology Inc, USA), rabbit monoclonal anti-GPX4 (1:1000, ab125066, Abcam, USA), and rabbit monoclonal anti-VINCULIN (1:1000, ab129002, Abcam, USA). The primary antibodies

were detected using secondary anti-rabbit or anti-mouse horseradish peroxidase-conjugated IgG. Bands were visualized by enhanced chemiluminescence developed by the ChemiDoc Imaging System (BioRad). Densitometry analysis was performed using ImageJ software.

1.8. Histology

Tissues were routinely processed, embedded in paraffin blocks and sectioned at 5μm thickness. A standard hematoxylin and eosin (H&E) (Azer Scientific; Catalogue numbers: ES36001 and ES36111) stain was performed, as well as a Pearl's Prussian blue stain (in house reagents: 1% Hydrochloric acid, 2% Potassium Ferrocyanide, 0.1% Nuclear Fast Red) for iron and a picrosirius red stain (Polysciences; Catalogue numbers: 24901A-500 and 24901B-500) for collagen.. The tissue sectioning, histochemical and immunohistochemical staining, and whole slide scanning were performed by members of the Penn Vet Comparative Pathology Core Facility (RRID:SCR_022438) at the University of Pennsylvania, PA, USA. The scanner used for whole slide imaging and the image analysis software was supported by an NIH Shared Instrumentation Grant (S10 OD023465-01A1). The Leica BOND RXm instrument used for IHC was acquired through the Penn Vet IIZD Core pilot grant opportunity 2022.

For the image quantification of the Sirius red and Pearl's Prussian blue stain, a total of 10 non-overlapping random images per mouse (n=5 per group) were analyzed using ImageJ software. The percentage of iron deposits and Sirius Red-positive areas was calculated by splitting each image, captured at 20X magnification, into its red, green, and blue (RGB) channels. Thresholds were then set to quantify the color intensity corresponding to the area fraction using ImageJ. For the 4-hydroxynonenal (4-HNE) staining, immunohistochemistry (IHC) micrographs

underwent a color deconvolution process using the ImageJ software, which separates brightfield images into channels representing the absorbance of individual dyes, including the brown DAB stain. After splitting the channels, the images were converted to grayscale, and the threshold tool was applied to determine the fraction of positive areas. Histopathologic anomalies for the H&E stained images were assessed using the NAFLD Activity Score (NAS) according to NIH guidelines. NAS evaluates liver sections to quantify disease severity based on three key components: steatosis, lobular inflammation, and hepatocellular ballooning.

1.9. Immunohistochemistry

For the immunohistochemistry performed at the American University of Beirut (AUB), formalin-fixed liver tissues were embedded in paraffin blocks, sectioned into 6μm slices, and mounted onto glass slides. The sections were then deparaffinized by immersing them in xylene and subsequently rehydrated through a graded series of ethanol washes. After rinsing in distilled water, the sections were subjected to antigen retrieval by immersion in a citrate buffer (0.1 M citric acid, 0.1 M sodium citrate, with drops of 2N sodium hydroxide (NaOH) added to distilled water) for one hour in a boiling water bath. Following retrieval, the slides were allowed to cool to room temperature and air-dry. Subsequent washes in distilled water and 1X PBS were conducted according to protocol. To block endogenous peroxidase activity, the sections were treated with a Peroxidase Block solution, followed by incubation with a protein block to reduce nonspecific binding. The sections were then incubated overnight with a primary antibody solution containing normal goat serum (NGS), 1X Triton, BSA, 1X PBS, and rabbit polyclonal anti-CYP4A antibody (diluted 1:150, Abcam). The following day, after thorough washes with 1X PBS, the sections were incubated with either the post-primary reagent and Novolink Polymer. The slides were then

exposed to 3,3'-diaminobenzidine (DAB) working solution (DAB Chromogen mixed with Novolink DAB Substrate Buffer) under dim light to develop the chromogenic signal. After additional washing in distilled water, the sections were counterstained with 0.1% hematoxylin, rinsed, dehydrated, and mounted for analysis. The stained sections were examined under a light microscope (137).

For the IHC performed in the U.S., 5 µm thick paraffin sections were mounted on ProbeOn™ slides (Thermo Fisher Scientific). The immunostaining procedure was performed using a Leica BOND RXm automated platform combined with the Bond Polymer Refine Detection kit (Leica #DS9800). Briefly, after dewaxing and rehydration, sections were pretreated with the epitope retrieval BOND ER2 high pH buffer (Leica #AR9640) for 20 minutes at 98°C. Endogenous peroxidase was inactivated with 3% H2O2 for 10 minutes at RT. Nonspecific tissue-antibody interactions were blocked with Leica PowerVision IHC/ISH Super Blocking solution (PV6122) for 30 minutes at RT. The same blocking solution also served as a diluent for the primary antibody. Rabbit primary antibodies against cleaved caspase-3 (CST, #9661) and 4 hydroxynonenal (HNE; Alpha Diagnostic International, #HNE11-S) were used at a concentration of 1/4000 and 1/500 respectively. The primary antibody solutions were incubated on the sections for 45 minutes at roomctemperature. A biotin-free polymeric IHC detection system consisting of HRP-conjugated goat anti-rabbit IgG (Vector Laboratories MP-7444) was then applied for 25 minutes at RT. Immunoreactivity was revealed with the DAB chromogen reaction. Slides were finally counterstained in hematoxylin, dehydrated in an ethanol series, cleared in xylene, and permanently mounted with a resinous mounting medium (Thermo Scientific ClearVueTM coverslipper). Sections of normal mouse lymphoid tissue and testes were included as positive

controls for Caspase 3 and 4HNE, respectively. Negative controls were obtained either by omission of the primary antibody or replacement with an irrelevant isotype-matched rabbit monoclonal antibody. All slides were finally scanned at 20X magnification using the Aperio Versa 200 whole slide scanner (Leica Biosystems, Buffalo Grove, Illinois). The images were then visualized with the Aperio ImageScope software (Leica Biosystems, Buffalo Grove, Illinois).

1.10. Measurement of 20-HETE Levels

Hepatic 20-HETE levels were quantified in isolated microsomes using HPLC (140). The procedure began by drying [1-14C]-labeled arachidonic acid (50–100 μmol/l) and reconstituting it in a reaction mixture containing 30 mmol/l isocitrate, 50 μg microsomes, and 0.2 units of isocitrate dehydrogenase in a reaction buffer (composed of 100 mmol/l potassium phosphate, pH 7.4, 5 mmol/l magnesium chloride, and 1 mmol/l EDTA). After a 5-minute incubation at 37°C, NADPH was introduced to initiate the reaction. Aliquots were collected at 30, 60, and 90 minutes, and the reaction was terminated by adding 100% methanol. The samples were then centrifuged to pellet the precipitated proteins, which were then stored at −20°C. Separation of the metabolites was conducted via HPLC on a C-18 column, utilizing an acetonitrile/water gradient, with identification achieved through coelution with labeled standards.

1.11. Lipid Peroxidation Assay

In order to measure lipid peroxidation in liver tissue extracts, we used the Lipid Peroxidation malondialdehyde (MDA) Colorimetric Assay (ab118970, Abcam, USA) as per the manufacturer's instructions (141-144). Absorbance was then measured on a microplate reader at OD 532 nm and the MDA concentration was calculated using the below equation:

$$\text{MDA Concentration} = (A / [\text{mg or mL}]) \times 4 * \times D = \text{nmol/ml or nmol/mg}$$

Where:

A = Amount of MDA in sample calculated from the standard curve (nmol).
mg = Original tissue amount used (e.g. 10 mg).
mL = Original plasma volume used (0.020 mL).
4* = Correction for using 200 µL of the 800 µL Reaction Mix.
D = Sample dilution factor if sample is diluted to fit within the standard curve range (prior to the reaction well set up).

1.12. Glutathione (GSH) Assay

The GSH Assay Kit (Colorimetric) (ab239709, Abcam, USA) was used as a colorimetric method for analyzing the total glutathione levels in samples using a microtiter plate reader (145-147). Liver tissues were homogenized and processed as per manufacturer's instructions. The assay is based on the glutathione recycling system by DTNB and glutathione reductase. DTNB and GSH react to generate 2-nitro-5-thiobenzoic acid which has a yellow color. Therefore, GSH concentration was determined by measuring absorbance at 412 nm. Total GSH levels were detrimental as follows: Total GSH = (O.D.sample - O.D.blank)/SlopeSTD Curve.

1.13. Caspase 3 Assay

We assessed caspase-3 activity, a key enzyme in the apoptotic process, using a colorimetric caspase-3 activity enzyme-linked immunosorbent assay (ELISA) kit (ab39401, Abcam, USA) (148-151). Liver tissue samples were homogenized in Cell Lysis Buffer (pH 7.5), and the homogenates were centrifuged at 10,000 x g for 1 minute to obtain the supernatant. A 50µl aliquot of this supernatant was used to prepare the sample according to the manufacturer's instructions. Protein concentrations were accurately determined using the BCA Protein Assay kit, as per the provided protocol. For the assay, 50µl of 2x Reaction Buffer (with 10mM dithiothreitol) and 5µl of the 4mM DEVD-p-NA substrate were added to each sample. The mixture was incubated at 37°C for 120 minutes. The absorbance was measured at OD 400 nm using a microplate reader. Caspase-3 activity levels in each group were expressed as fold change relative to the control (wild type) group.

1.14. Statistical Analysis

Statistical analysis was performed using GraphPad Prism Software (10.2.3, CA, USA). All the data was initially checked for outliers. Normality and Lognormality test was then performed to assess the distribution of the data (Shapiro-Wilk normality test, and Kolmogorov-Smirnov normality test). If the samples followed a normal distribution, an ordinary one way analysis of variances (ANOVA) test was performed followed by Tukey's posttest in order to determine the significance, where p value ≤ 0.05 is considered statistically significant. If the data did not follow a normal distribution, a non-parametric Kruskal-Wallis test was performed. All of the results were expressed as mean ± standard deviation (SD).

2. Clinical Study

2.1. Study Design and Subjects

In an observational study we enrolled 50 individuals with β-thalassemia (30 TDT and 20 NTDT), alongside 20 healthy controls (healthy subjects). For the recruitment of patients, all adult β-thalassemia patients who are followed up regularly in the Rare Disease Center of the General Medicine Unit at Fondazione IRCCS Ca' Granda Ospedale Maggiore Policlinico and who have provided their consent were recruited.

2.2. Ethics Statement

All experiments were conducted according to the ethical policies and procedures approved by the ethical committee of Fondazione IRCCS Ca' Granda Ospedale Maggiore Policlinico in Milan, Italy (protocol # 95_2022bis). Informed consent was obtained from all study participants for the use of their blood samples and the review of their medical records. This included accessing their test results and relevant medical history, as well as clinical and demographic information.

2.3. Sample collection and storage

Blood samples were collected during the routine follow-up visit of the patients. Some of the blood samples were sent to the central lab for analysis of different clinical parameters, outlined briefly below:

- Hematological parameters: hemoglobin, hematocrit, mean cellular volume (MCV), RBCs, RBCs distribution width (RDW), reticulocytes, platelets, white blood count (WBC), neutrophils, and lymphocytes.
- Liver Function Tests: alanine transaminase (ALT), aspartate transaminase (AST), gamma-glutamyl transferase (GGT), and alkaline phosphatase (ALP).
- Iron parameters: serum ferritin, transferrin, serum iron, transferrin saturation (TSAT)
- Renal Function Tests: blood urea nitrogen (BUN), Creatinine

The remaining blood was collected and immediately centrifuged to separate its components into plasma, serum and buffy coat. Plasma and serum samples were stored at -80 °C until used for different biochemical assays. The buffy coat was carefully isolated, stored at -20 °C and reserved for genetic studies.

2.4. Quantification of NTBI Levels

Serum NTBI content was measured using HPLC (36). Serum samples were collected and stored at -80˚C until analysis. For the assay, 50 µl of 800 mM nitrilotriacetic acid (NTA) solution (pH 7.0) was added to 450 µl of serum. The mixture was incubated at room temperature for 20 minutes, allowing the excess NTA to chelate iron that was non-specifically bound to serum proteins and low-molecular-weight ligands, forming a Fe-[NTA] complex. This solution was then ultrafiltered using an Amicon Centricon 30 microconcentrator (Amicon Corporation, Lexington, MA, USA) at 13,000 x g for 30 minutes. A 20 µl aliquot of the ultrafiltrate was injected into a metal-free HPLC system (PerkinElmer® Series 200™ IC titanium pump module; Perkin-Elmer Life Science, Boston, MA, USA).

The HPLC assay was performed on a reverse-phase C18 column (4 µm, 3.9 x 150 mm; Waters, Milford, MA, USA) using an isocratic mobile phase consisting of 20% acetonitrile and 3

mM CP22 (3-hydroxy-1-propyl-2-methyl-pyridine-4-one) in 5 mM sodium phosphate buffer (Na2HPO4-NaH2PO4), adjusted to pH 7.0 (Schrier SL, 1994). CP22 has a high affinity for iron and forms an orange-colored Fe-[CP22]3 complex from the Fe-[NTA] complex, which was detected at 450 nm. Iron concentrations were determined by comparison with a calibration curve. The NTBI retention time under these conditions was 4.6 minutes.

Iron standards ranging from 0 to 10 μM were prepared from a stock Fe-[NTA] solution and diluted with Milli-Q distilled water (Millipore, Bedford, MA, USA). This iron-free water was also used as the blank. Standards were routinely run in 1 μM increments, and 20 μl of each standard or blank was injected into the HPLC system. The iron content measured in the blank was then subtracted from the values obtained for the Fe-[NTA] standards to correct for background levels.

The NTBI assay was also performed on serum samples from healthy control subjects. In normal individuals, NTBI values are typically negative, as the assay measures samples alongside a corresponding blank containing water and NTA. The small amounts of iron in water, not bound by transferrin, result in negative NTBI values after blank subtraction, as transferrin in the samples partially captures iron from the Fe-[NTA] complex.

2.5. Assessment of MDA Levels

The LPO-586™ assay (OxisResearch™) was used to measure MDA levels in serum samples according to instructions by the manufacturer (152-154). This assay is based on the reaction of a chromogenic reagent, N-methyl-2-phenylindole (R1), with MDA at 45°C. One molecule of MDA reacts with 2 molecules of reagent R1 to yield a stable chromophore with

maximal absorbance at 586 nm. Using data from the yielded standard curve, the concentration of MDA was calculated.

2.6. Detection of intracellular superoxide levels using HPLC

The measurement of DHE-derived oxidation products, indicating ROS production, in plasma samples was performed using HPLC (138, 139). This method is very sensitive and reliable in detecting superoxide anions compared to immunofluorescent DHE staining and other ROS detection methods. In brief, plasma samples were incubated for 30 min with 50 μM DHE (Sigma-Aldrich) in HBSS–100 μM DTPA. After incubation, they were centrifuged at 12,000 x g for 10 minutes at 4°C, and then dried under vacuum. The samples were subsequently analyzed using HPLC with fluorescence detection. The concentrations of DHE, EOH, and ethidium products were quantified by comparing the integrated peak areas of the obtained chromatograms with those of standard curves for each product, under identical chromatographic conditions. EOH and ethidium were detected by fluorescence with excitation at 510 nm and emission at 595 nm, while DHE was monitored by ultraviolet absorption at 370 nm. The results were expressed as the amount of EOH produced (in nmol) normalized to the amount of DHE consumed (i.e., the initial DHE minus the remaining DHE in the sample, expressed in μmol).

2.7. Measurement of 20-HETE Levels

Plasma 20-HETE levels in humans were quantified in isolated microsomes using HPLC. The procedure began by drying [1-14C]-labeled arachidonic acid (50–100 μmol/l) and reconstituting it in a reaction mixture containing 30 mmol/l isocitrate, 50 μg microsomes, and 0.2 units of isocitrate dehydrogenase in a reaction buffer (composed of 100 mmol/l potassium

phosphate, pH 7.4, 5 mmol/l magnesium chloride, and 1 mmol/l EDTA). After a 5-minute incubation at 37°C, NADPH was introduced to initiate the reaction. Aliquots were collected at 30, 60, and 90 minutes, and the reaction was terminated by adding 100% methanol. The samples were then centrifuged to pellet the precipitated proteins, which were then stored at −20°C. Separation of the metabolites was conducted via HPLC on a C-18 column, utilizing an acetonitrile/water gradient, with identification achieved through coelution with labeled standards.

2.8. Assessment of genetic polymorphisms in the CYP4A, and CYP4F genes

DNA was isolated from the collected buffy coat using the Maxwell® 16 Blood DNA Purification Kit (Promega Corporation, USA) according to manufacturer's protocol (155-157) and its concentration was measured using the Nanodrop 1000 (ThermoFisher Scientific, USA). Genotyping was then assessed by RT-PCR on the 7500 Real Time PCR System (ThermoFisher Scientific, USA), using the GoTaq® Probe System (Promega Corporation, USA) and specific TaqMan™ SNP Genotyping Assay probes (ThermoFischer Scientific,USA), the characteristics of which are listed in **Table 2**. Allelic discrimination analysis was performed with the GT module software of ThermoFisher Cloud (2020.1.4-Q1-20-build1).

Table 2. Characteristics of the TaqMan™ SNP Genotyping Assay Probes used based known functional SNPs of CYP4A and CYP4F genes

Gene	SNP	Type	Polymorphism	Location on Chromosome
CYP4A11	rs1126742	Intron	A/G	1p33
CYP4A11	rs9333025	Intron	C/T	1p33
CYP4F2	rs3093135	Intron	A/T	19p13.12
CYP4F2	rs2108622	Intron	C/T	19p.13

2.9. Statistical Analysis

Discrete and continuous variables were presented as absolute frequencies and relative percentages, or as means (± SD) or medians (minimum-maximum), respectively. The pairwise Spearman correlation was calculated to assess the relationships between plasma 20-HETE levels and other factors, including oxidative stress markers and iron parameters. Differences in the distribution of factors were evaluated using the nonparametric Wilcoxon-Mann-Whitney test for two groups and the Kruskal-Wallis test for three or more groups. Additionally, the distribution of the same parameters between healthy individuals and patients with β-thalassemia was analyzed using the Wilcoxon-Mann-Whitney and Kruskal-Wallis tests. All analyses were conducted using Stata 18 (StataCorp, 2023. Stata Statistical Software: Release 18. College Station, TX: StataCorp LLC).

RESULTS

1. Animal Study

1.1.HET0016 administration reduced liver-to-body weight ratio in Hbb$^{th3/+}$ mice without affecting spleen-to-body weight ratio or hematological parameters

The administration of HET0016 in Hbb$^{th3/+}$ mice led to a significant reduction in the liver-to-body weight ratio **(Figure 9-A)**. Additionally, the liver of HET0016-treated Hbb$^{th3/+}$ mice displayed a slightly healthier and brighter-looking red color compared to their untreated counterparts **(Figure 9-B)**. However, despite the observed effect on liver, HET0016 administration did not lead to any changes in the spleen-to-body weight ratio or overall spleen size in Hbb$^{th3/+}$ mice **(Figure 9-C-D).** Furthermore, the hematological parameters, including hemoglobin, hematocrit, red blood cell count, nucleated red blood cells, reticulocytes, platelets, mean corpuscular volume, mean corpuscular hemoglobin, mean corpuscular hemoglobin concentration, and coefficient of variation in red cell distribution width, did not improve, and remained unaffected by HET0016 treatment **(Figure 9-E-M)**.

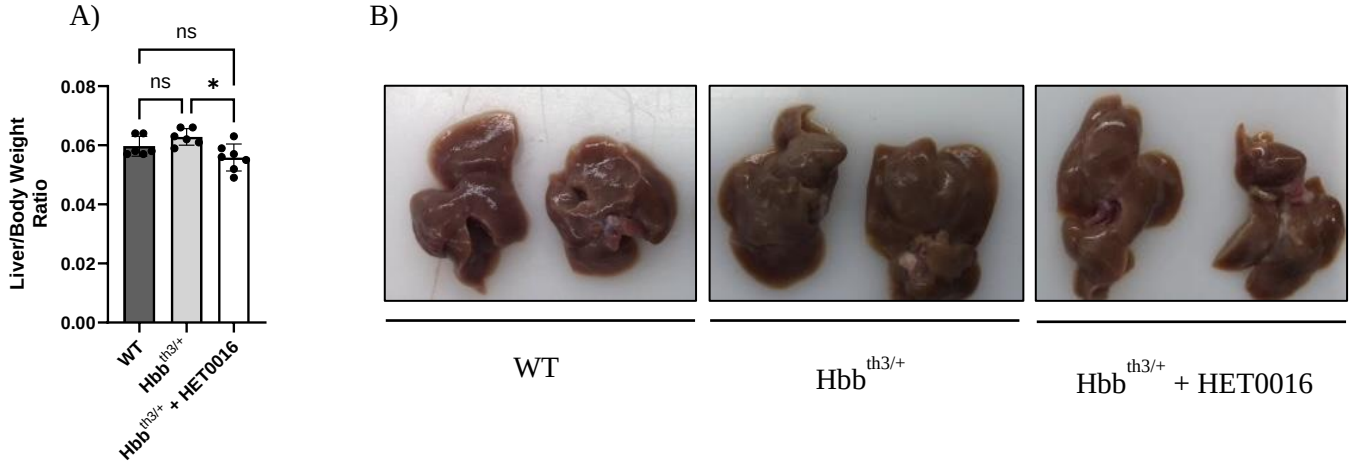

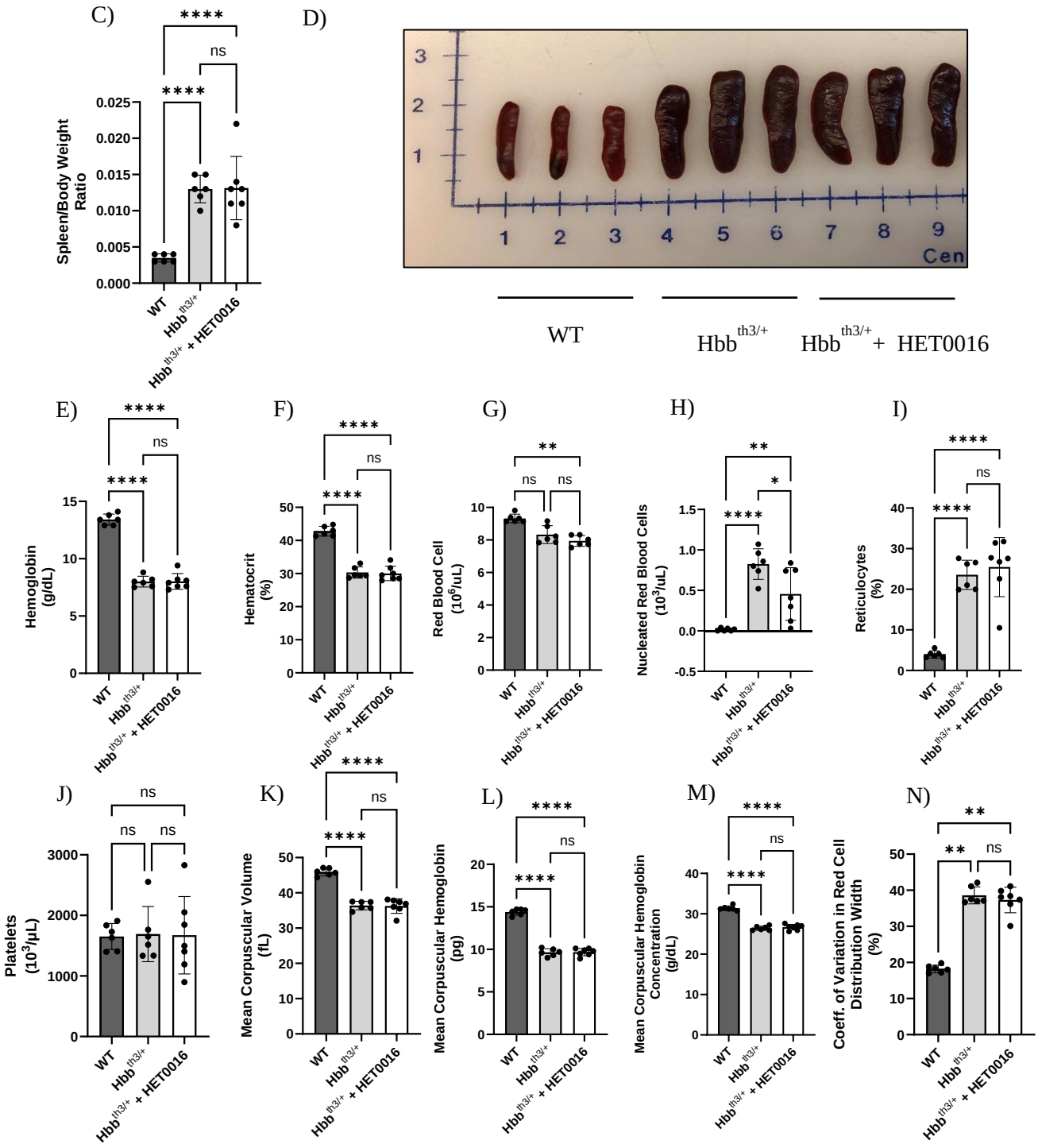

Figure 9: HET0016 administration reduced liver-to-body weight ratio in Hbb$^{th3/+}$ mice without affecting spleen-to-body weight ratio or hematological parameters. (A-B) Liver-to-body weight ratio and representative image of the gross appearance of the livers, (C-D) spleen-to-body weight ratio and representative images of the gross appearance and size of the spleens, and (E-N) RBC parameters. Values represented as mean ± SD. WT (n=6), Hbb$^{th3/+}$ (n = 6) and Hbb$^{th3/+}$ + HET0016 (n=7); Groups were tested either using the ordinary one way-ANOVA test

or the non-parametric one way-ANOVA analyses (Kruskal Wallis Test); * $p \leq 0.05$, ** $p \leq 0.01$, *** $p \leq 0.001$, ****$p \leq 0.0001$;ns: non-significant.

1.2. HET0016 administration reduced intracellular ROS levels and NADPH Oxidase activity in Hbb$^{th3/+}$ mice

Superoxide production in liver tissues was significantly increased in *Hbb$^{th3/+}$ mice* compared to their control littermates. This increase was mitigated by HET0016 administration **(Figure 10-A)**. Additionally, the rise in ROS levels was associated with increased NADPH oxidase activity, which also showed a significant reduction following HET0016 treatment **(Figure 10-B)**.

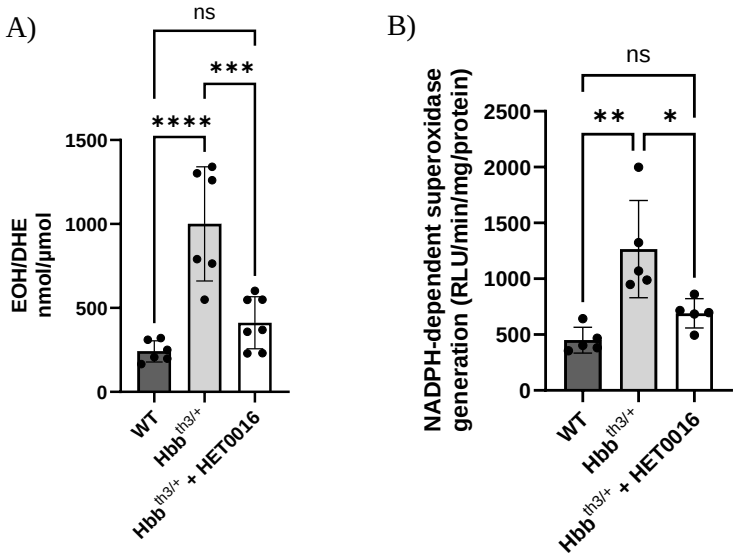

Figure 10: HET0016 administration reduced intracellular ROS levels and NADPH Oxidase activity in Hbb$^{th3/+}$ mice. (A) HPLC analysis and quantification of EOH/DHE ratios (nmol/umol), and (B) NADPH-dependent superoxide generation (RLU/min/mg protein) measured in liver tissues of the different groups of mice. Values represented as mean ± SD. WT (n=5-6), Hbb$^{th3/+}$ (n = 5-6) and Hbb$^{th3/+}$ + HET0016 (n=5-7); Groups were tested using the ordinary one way-ANOVA test * $p \leq 0.05$, ** $p \leq 0.01$, *** $p \leq 0.001$, ****$p \leq 0.0001$; ns: non-significant

1.3. HET0016 decreased Cyp4a10, and Cyp4a14 mRNA expression levels, Cyp4a14 protein levels, and 20-HETE levels in Hbb$^{th3/+}$ mice

Significant changes were observed in the mRNA expression levels of Cyp4a10 and Cyp4a14 in Hbb$^{th3/+}$ mice compared to controls, with both decreasing following HET0016 administration **(Figure 11-A-B)**. Additionally, there was a statistically significant increase in CYP4A14 protein levels in the livers of Hbb$^{th3/+}$ mice compared to controls, which also decreased with HET0016 treatment **(Figure 11-C-D).** The efficacy of HET006 in reducing CYP4A levels in the liver was further confirmed through IHC staining **(Figure 11-E)**. Finally, 20-HETE activity was elevated in Hbb$^{th3/+}$ mice relative to controls, which is consistent with the increased expression of their corresponding CYPs, and this activity was significantly reduced with HET0016 administration **(Figure 11-F)**.

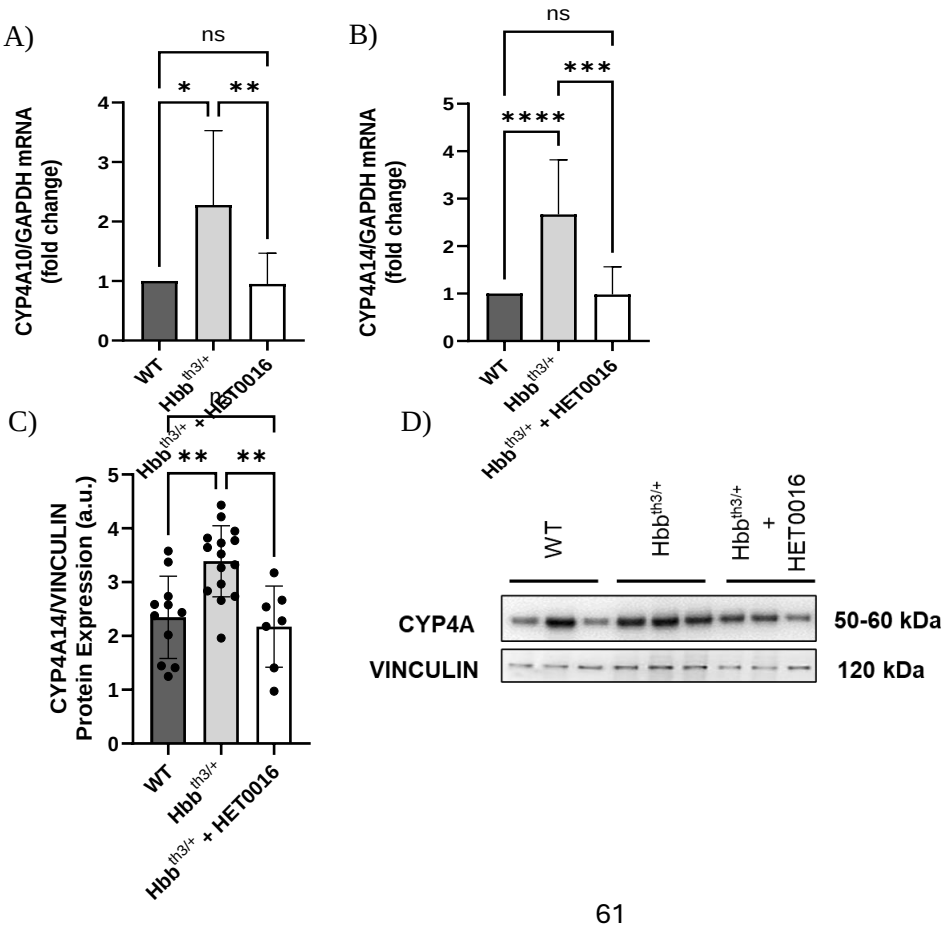

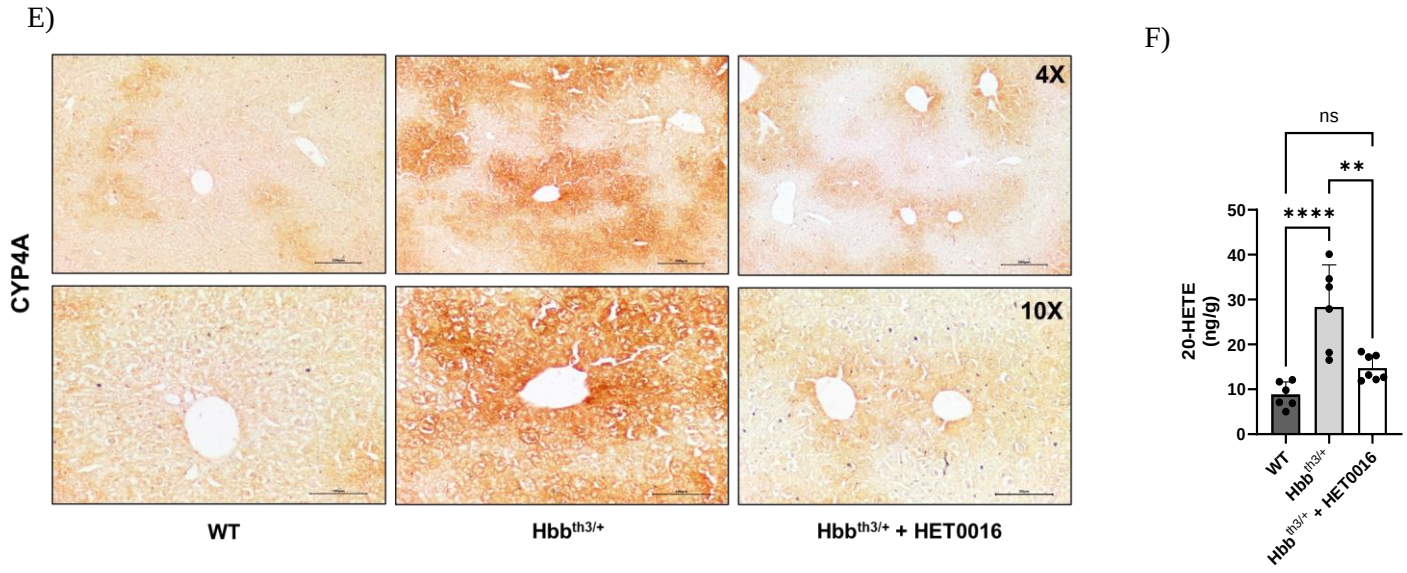

Figure 11: HET0016 decreased Cyp4a10, and Cyp4a14 mRNA expression levels, Cyp4a14 protein levels, and 20-HETE levels in Hbb$^{th3/+}$ mice. (A-B) Cyp4a10, and Cyp4a14 mRNA expression levels calculated as a fold change using the ΔΔCt method, (C) Representative western blot showing the expression of CYP4A in addition to CYP4A/VINCULIN quantification, (D) Representative figure of IHC staining for CYP4A at 4X and 10X and (E) Assessment of 20-HETE activity (metabolite produced by CYP4A) by HPLC. Values represented as mean ± SD. WT (n=11), Hbb$^{th3/+}$ (n = 15) and Hbb$^{th3/+}$ + HET0016 (n=7); Groups were tested using either the ordinary one way-ANOVA test or the non-parametric one way-ANOVA analyses (Kruskal Wallis Test); * $p \leq 0.05$, ** $p \leq 0.01$, *** $p \leq 0.001$, ****$p \leq 0.0001$; ns: non-significant

1.4. Treatment with HET0016 decreased lobular inflammation, and ballooning of hepatocytes in Hbb$^{th3/+}$ mice

Hematoxylin and eosin staining of liver tissues from Hbb$^{th3/+}$ mice revealed signs of interstitial and perivascular inflammation in addition to hepatocytic ballooning. These pathological features were markedly improved following treatment with HET0016 **(Figure 12)**. Quantitative analysis of these histological changes, as reflected in the NAS activity score, further confirmed the therapeutic effect of HET0016 **(Table 3)**.

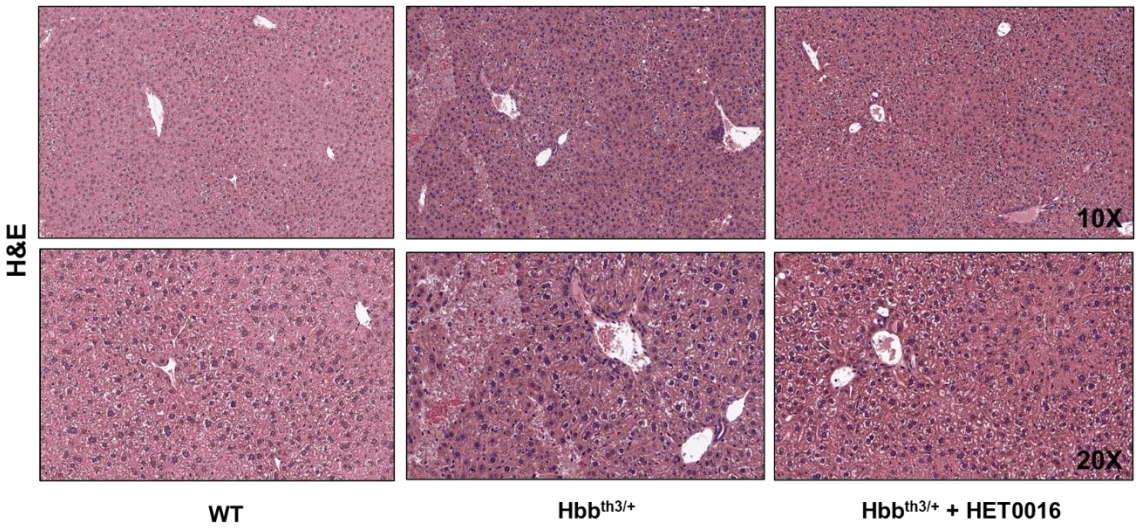

Figure 12. Treatment with HET0016 decreased lobular inflammation, and ballooning of hepatocytes. Representative images taken at 10X and 20X are shown.

Table 3. The calculated NAFLD activity score (NAS). WT (n=5), $Hbb^{th3/+}$ (n = 5) and $Hbb^{th3/+}$ + HET0016 (n=5).

Groups	Steatosis (0-3)	Lobular Inflammation (0-3)	Hepatocellular Ballooning (0-2)	Total NAS Score (0-8)
WT	0	0	0	0
$Hbb^{th3/+}$	0	2	2	4
$Hbb^{th3/+}$ + HET0016	0	1	1	2

1.5. Treatment with HET0016 reduced fibrosis, and lipid peroxidation in Hbb$^{th3/+}$ mice

Sirius red staining, which is used to detect and visualize collagen fibers, indicated significant interstitial and perivascular fibrosis in the liver of Hbb$^{th3/+}$ mice. This fibrosis was substantially reduced with HET0016 administration **(Figure 13-A-B)**. Decreased mRNA expression levels of the liver injury marker HGF in Hbb$^{th3/+}$ mice treated with HET0016 also confirmed these findings **(Figure 13-C)**. We then assessed the impact of HET0016 on the accumulation of lipid peroxides in the liver of Hbb$^{th3/+}$ mice. Treatment with HET0016 significantly attenuated increased levels of the lipid peroxidation markers MDA and 4-HNE in Hbb$^{th3/+}$ mice **(Figure 13-D-F).**

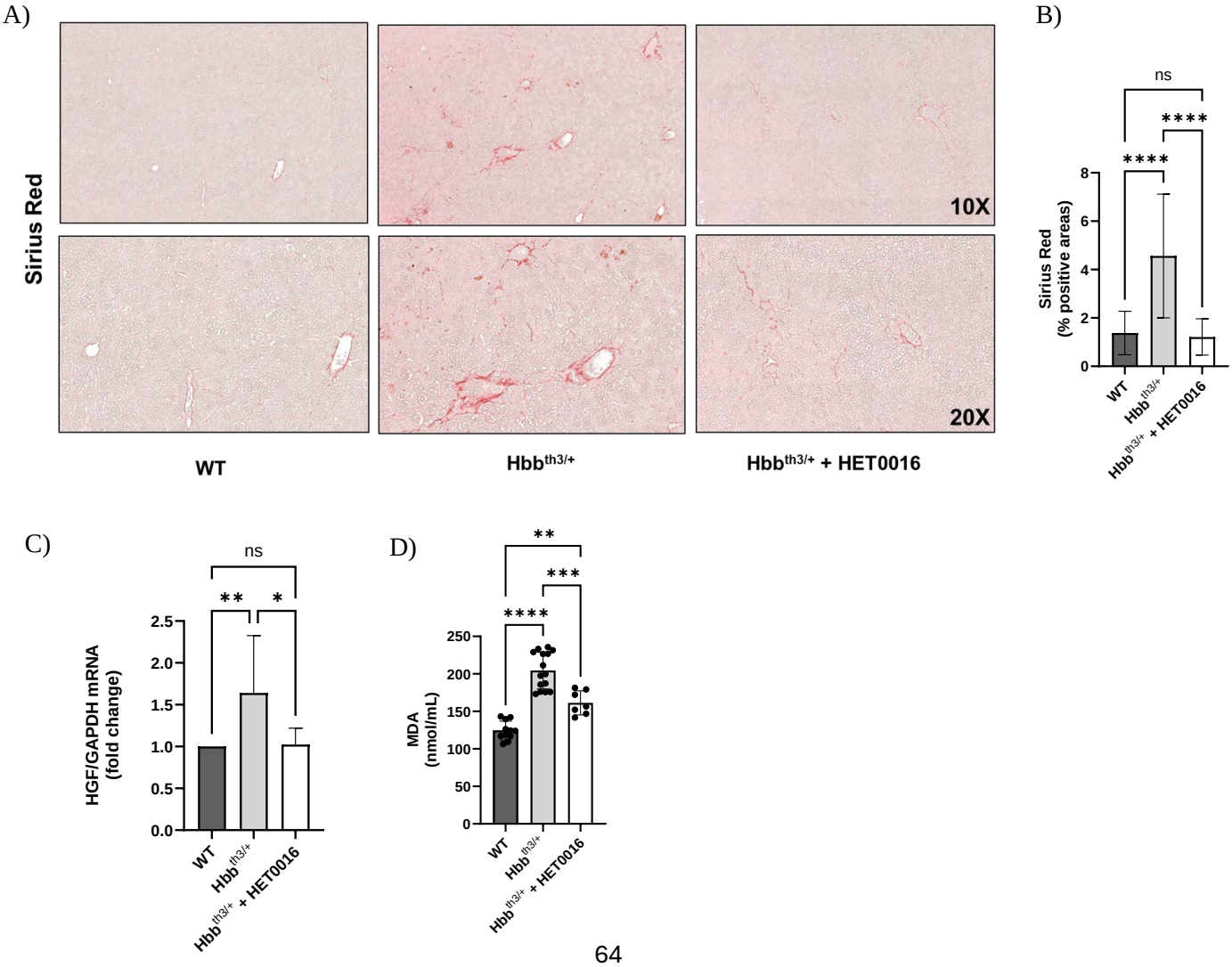

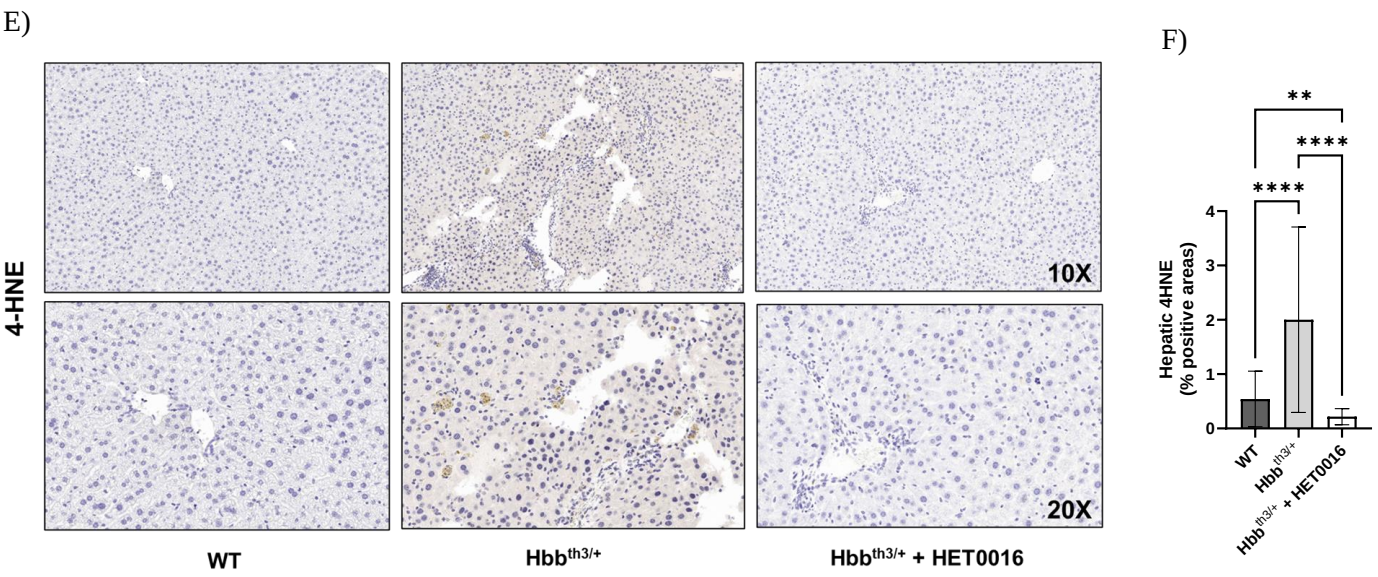

Figure 13: Treatment with HET0016 reduced fibrosis, and lipid peroxidation in Hbb$^{th3/+}$ mice. (A) Representative figure of Sirius red stain at 10X and 20X, and (B) Corresponding quantification of images (n=5/group), (C) HGF mRNA expression levels calculated as a fold change using the ΔΔCt method, (D) MDA Assay, (E) Representative of IHC staining for 4-HNE at 10X and 20X and (F) corresponding quantification of images (n=5/group). Values represented as mean ± SD. WT (n=11), Hbb$^{th3/+}$ (n = 15) and Hbb$^{th3/+}$ + HET0016 (n=7); Groups were tested using the ordinary one way-ANOVA test. * $p \leq 0.05$, ** $p \leq 0.01$, *** $p \leq 0.001$, ****$p \leq 0.0001$; ns: non-significant

1.6. Treatment with HET0016 reduced apoptosis in Hbb$^{th3/+}$ mice

The observed increase in markers of inflammation, fibrosis, and lipid peroxidation in the liver can be strongly associated with enhanced apoptosis and cell death. Notably, treatment with HET0016 significantly reduced apoptosis in Hbb$^{th3/+}$ mice, as demonstrated by the immunohistochemistry results in **Figure 14-F** and further confirmed by the Caspase-3 activity assay shown in **Figure 14-G**. These findings suggest that HET0016 could effectively mitigate the apoptotic pathways linked to liver injury in Hbb$^{th3/+}$ mice.

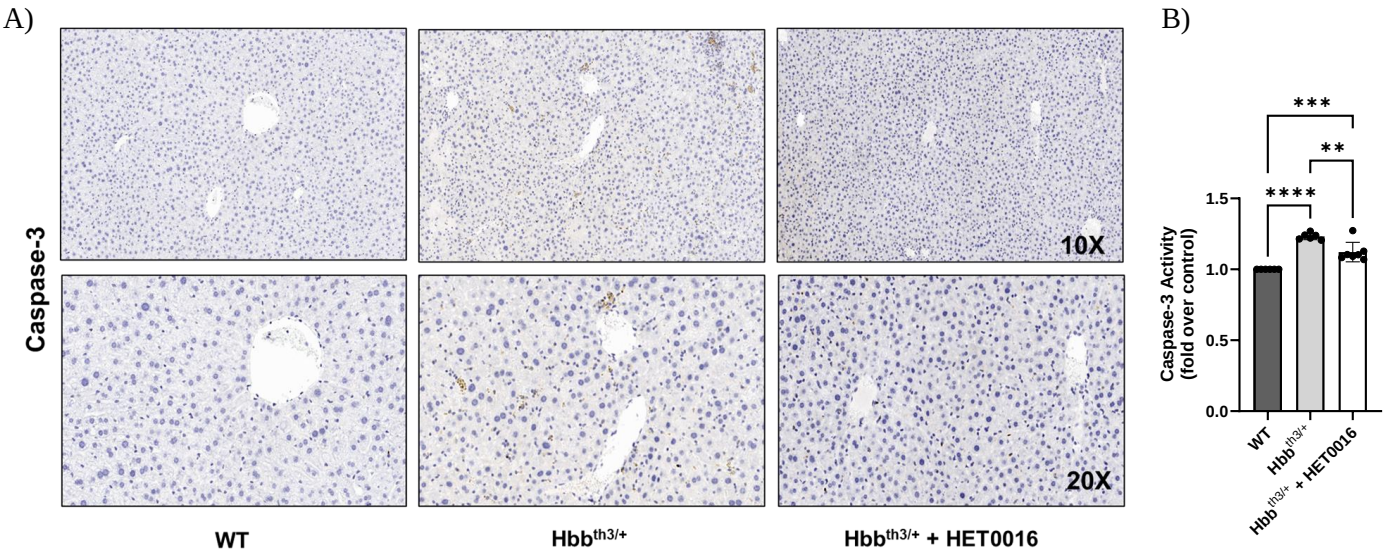

Figure 14. Treatment with HET0016 reduced apoptosis in Hbb$^{th3/+}$ mice. (A) Representative figure of IHC staining for Caspase 3 at 10X and 20X, and (B) Caspase 3 activity. Values represented as mean ± SD. WT (n=6), Hbb$^{th3/+}$ (n = 6) and Hbb$^{th3/+}$ + HET0016 (n=7); Groups were tested using the ordinary one way-ANOVA test. * $p \leq 0.05$, ** $p \leq 0.01$, *** $p \leq 0.001$, ****$p \leq 0.0001$; ns: non-significant

1.7. HET0016 decreases iron and inhibits ferroptosis in Hbb$^{th3/+}$ mice

We then assessed the effect of HET0016 on iron using Perls' Prussian blue staining. The number of iron-positive cells was counted and compared across the different mouse groups. As shown in **Figure 15-A-B**, treatment with HET0016 significantly reduced iron in the liver of Hbb$^{th3/+}$ mice. This finding prompted us to look at the ferroptosis pathway. Specifically, we examined the effects of 20-HETE inhibition on the mRNA and protein expression levels of glutathione peroxidase 4 (GPX4), a central regulator that serves to inhibit ferroptosis. As shown in **Figure 15-C-E**, HET0016 significantly increased GPX4 expression. Moreover, treatment with HET0016 attenuated the decreases in total GSH levels, which acts as a cofactor of GPX4 **(Figure 15-F)**.

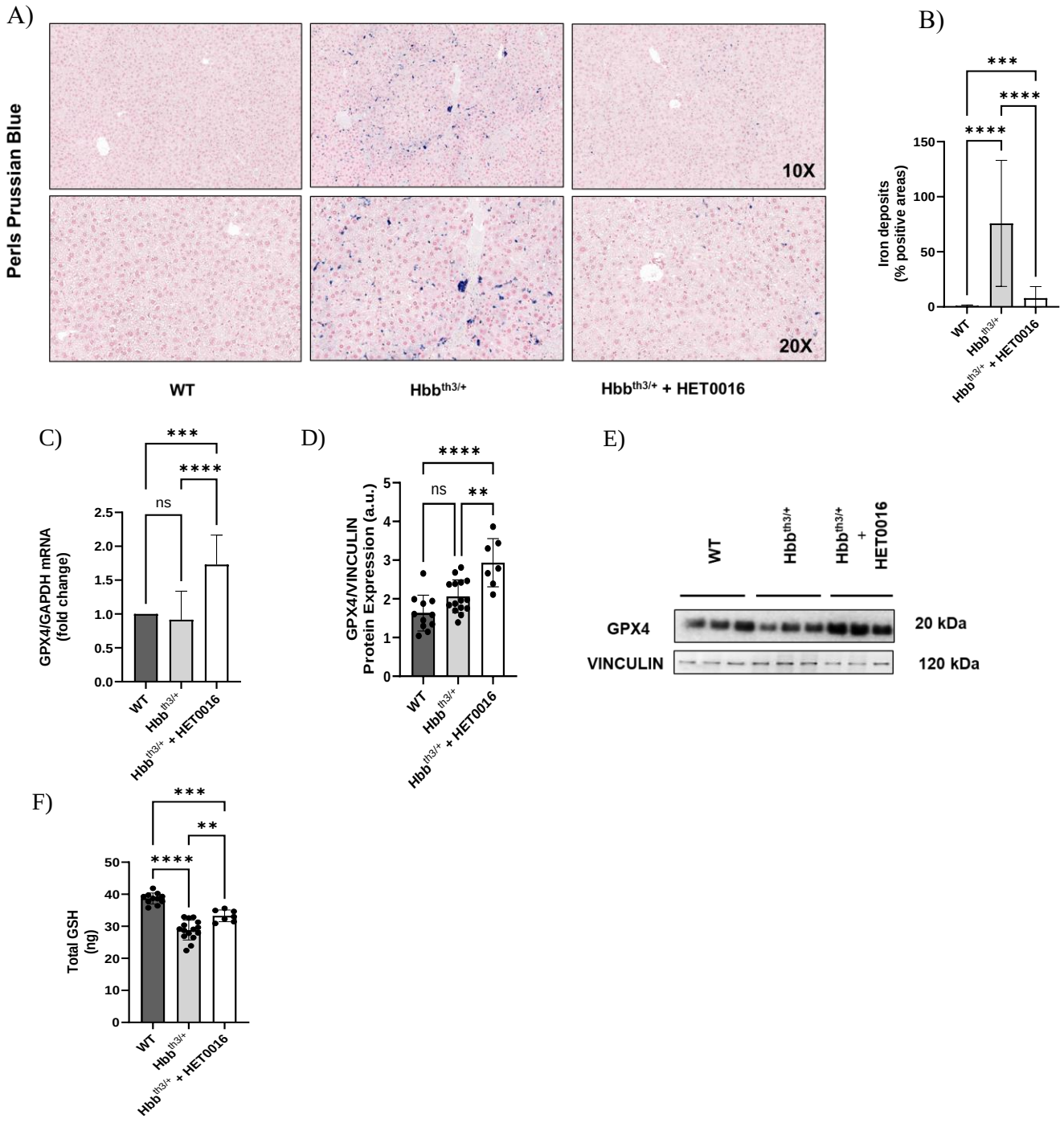

Figure 15. HET0016 decreases iron and inhibits ferroptosis in Hbb$^{th3/+}$ mice. (A) Representative figure of Pearl's Prussian blue stain at 10X and 20X, and (B) Corresponding quantification of images (n=5/group), (C) GPX4 mRNA expression levels calculated as a fold change using the ΔΔCt method, (D-E) Representative western blot showing the expression of GPX4 in addition to GPX4/VINCULIN quantification, and (F) Total GSH Levels. Values represented as mean ± SD. WT (n=11), Hbb$^{th3/+}$ (n = 15) and Hbb$^{th3/+}$ + HET0016 (n=7); Groups were tested using the ordinary one way-ANOVA test. * $p \leq 0.05$, ** $p \leq 0.01$, *** $p \leq 0.001$, ****$p \leq 0.0001$; ns: non-significant

2. Clinical Study

2.1. Clinical Characteristics of the Study Subjects

The analysis of clinical characteristics related to iron and oxidative stress in our study subjects is presented in **Table 4,** highlighting the key differences among them. As shown, patients with β-thalassemia had significantly higher 20-HETE levels when compared to healthy individuals.

Table 4. Comparisons of Clinical Characteristics and 20-HETE levels between healthy subjects and β-Thalassemia patients.

Clinical Parameters	Healthy Subjects (n=20)	β-Thalassemia Patients (n=50)	p-value
Iron (mcg/dL)*	98.0 ± 33.5	224.2 ± 69.2	< 0.001
Serum Ferritin (mg/L)**	68.5 (22-374)	1222.8 (131-10,614)	< 0.001
Transferrin (mg/dL)	266.4 ± 33.2	181.0 ± 26.0	< 0.001
TSAT (%)	26.2 ± 9.3	88.0 ± 24.7	< 0.001
NTBI (µM)*	-0.8 ± 0.5	2.2 ± 2.1	< 0.001
MDA (µM)*	0.5 ± 0.2	0.9 ± 0.4	< 0.001
ROS-DHE*	126.8 ± 37.6	795.6 ± 138.4	< 0.001
20-HETE*	13.6 ± 2.5	26.0 ± 4.0	< 0.001

*Values represented as mean ± SD. **Values are presented as median and range.

A sub analysis study on the cohort of β-thalassemia patients on certain treated modalities for their basic disease or for the prevention of certain complications also revealed differences among 20-HETE levels. These have been summarized in **Table 5**.

Table 5. 20-HETE levels among β-thalassemia patients on certain treatment modalities.

Treatment Modality	20-HETE	p-value
Splenectomy		
Yes (n=30)	26.3 ± 3.8	0.458
No (n=20)	25.5 ± 4.2	
Hydroxyurea		
Yes (n=9)	23.8 ± 2.6	0.055
No (n=41)	26.5 ± 4.1	
Transfusion		
Yes (n=40)	27.1 ± 3.6	< 0.001
No (n=10)	21.6 ± 1.4	
Chelation		
Yes (n=39)	23.0 ± 0.0	0.002
No (n=11)	26.8 ± 3.9	
Medications (aspirin, ACE inhibitors, ARBs, beta blockers, insulin)		
Yes (n=27)	25.1 ± 3.3	0.080
No (n=23)	27.1 ± 4.5	

Values represented as mean ± SD.

Furthermore, correlation studies in β-thalassemia patients revealed a strong association between 20-HETE levels and ROS-DHE levels, as well as a moderate correlation between 20-HETE levels and iron levels. **(Figure 16)**.

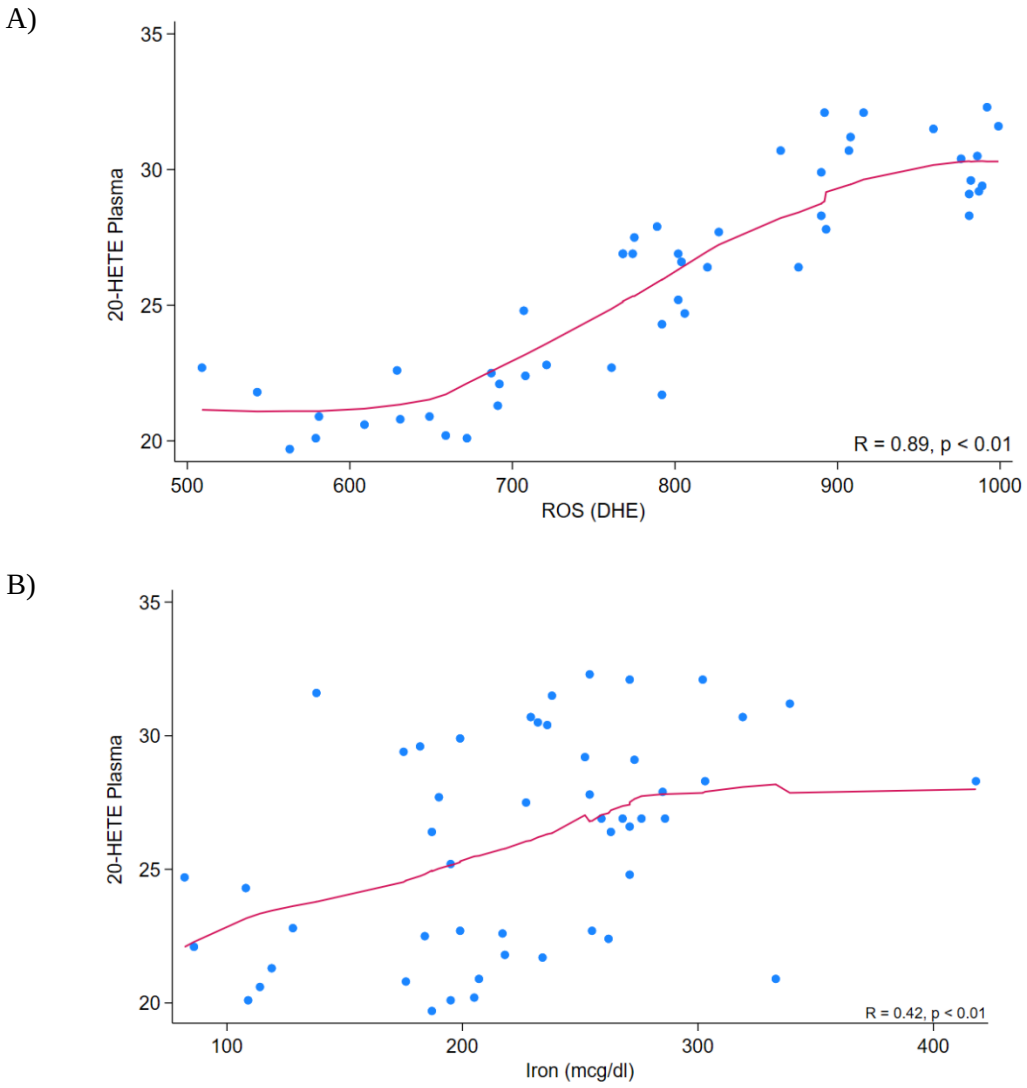

Figure 16. Correlation of 20-HETE with iron parameters and markers of oxidative stress. Representative figure showing a strong correlation between 20-HETE and (A) ROS-DHE levels, as well as a moderate correlation between 20-HETE and (B) iron levels in β-thalassemia patients. (n=50).

2.2. 20-HETE levels and its association with genotype distribution

As shown in **Table 6**, there were no significant associations between 20-HETE levels and any of the four polymorphisms tested (in all p value > 0.05).

Table 6. Association of 20-HETE Levels with Genotype Distribution in Patients

	20-HETE	*p-value*
rs9333025		
CC (n=37)	26.3 + 4.3	0.9695
CT (n=13)	25.9 + 3.1	
rs1126742		
AA (n=35)	25.7 + 4.1	0.4922
AG (n=14)	26.9 + 3.8	
GG (n=1)	22.8 + 0.0	
rs3093135		
AA (n=26)	27.0 + 3.9	0.1442
AT (n=22)	24.7 + 4.0	
TT (n=2)	26.7 + 0.4	
rs2108622		
CT (n=21)	26.3 + 3.9	0.8098
CC (n=24)	25.7 + 4.2	
TT (n=5)	26.0 + 3.7	

*Values represented as mean ± SD

DISCUSSION

Oxidative damage caused by ROS plays a crucial role in the cell injury and tissue damage observed in β-thalassemia patients. Recent studies have also shown that ROS generation in β-thalassemia is multifactorial, involving several mechanisms that contribute to its harmful effects (40, 41). Elevated ROS levels in various organs have been linked to numerous pathological outcomes, including inflammation, fibrosis, and apoptosis. Moreover, the sources of ROS production in pathophysiology have been proposed to be tissue and disease specific. Despite all advancements in the understanding of β-thalassemia, and to our knowledge, no study to date has identified specific sources of ROS, highlighting a critical gap in the field.

Iron chelation therapy is a cornerstone treatment for β-thalassemia. By sequestering both intracellular and extracellular iron, which catalyzes the production of harmful free oxygen radicals, iron chelators have emerged as effective general antioxidants by helping reduce oxidative stress and limit subsequent damage. However, while ROS are often implicated in injury and disease processes, they are also essential for normal cellular functions, including gene transcription, cell proliferation, and the regulation of blood flow and blood pressure. This dual role of ROS, balancing between necessary physiological functions and pathological damage, helps explain why attempts to treat ROS-related diseases using general antioxidants have often been unsuccessful. In some cases, the use of general antioxidants has even led to adverse outcomes, as they may disrupt vital ROS-dependent processes. This complexity underscores the need for more targeted therapeutic strategies in managing oxidative stress in red cells disorders and hemoglobinopathies in general, and in diseases like β-thalassemia specifically. In light of

this, we provide significant insights in this study for the first time into the role of CYP450 and the metabolite 20-HETE in oxidative stress production in β-thalassemia.

HET0016 has been explored for its effects on body weight and body-to-organ weight ratios, which are crucial indicators of systemic and organ-specific responses to disease and therapeutic interventions (158). By inhibiting 20-HETE, HET0016 has shown potential in reducing organ hypertrophy. In our study, the administration of HET0016 in $Hbb^{th3/+}$ mice resulted in a notable reduction in the liver-to-body weight ratio. This was accompanied by visible improvements in the overall gross appearance of the liver. These findings suggest that HET0016 could have beneficial effects on liver health in $Hbb^{th3/+}$ mice, likely through mechanisms related to its inhibitory effects on 20-HETE, which is known to contribute to liver inflammation, oxidative stress, and fibrosis. Thus, the reduction in liver weight could indicate a potential alleviation of liver hypertrophy or hepatomegaly, a common complication oberserved in β-thalassemia patients (159). In fact, one study by Park et al looked at the effect of HET0016 on diabetic pathophysiology in high fat diet (HFD) mice and also showed a reduction in liver size following treatment with HET0016 at a dose of 5 mg/kg/day intraperitoneally for 12 weeks (158). Similarly, a study by Yang et al. showed that HET0016 substantially improved alcoholic steatosis and alcohol-induced liver injury including the overall gross appearance of the organ (160).

Despite the positive effects on the liver, HET0016 administration did not affect the spleen-to-body weight ratio or spleen size, highlighting a degree of organ-specificity in the drug's mechanism of action. This is consistent with the fact that splenomegaly in β-thalassemia is primarily driven by ineffective erythoproesis and chronic hemolysis, mechanisms that may not be

directly influenced by 20-HETE inhibition. Furthermore, the absence of changes in hematological parameters indicate that HET0016 does not directly influence the anemic condition characteristic of β-thalassemia. The persistence of these hematological abnormalities after treatment suggests that while 20-HETE inhibition can mitigate liver pathology, it does not seem to correct the state of ineffective erythropoiesis or hemolysis-driving anemia in β-thalassemia. This is not surpridsing givren the mechanism of action of the drug which primarily acts on the liver and kidney. Whether long-term adminsitration of HET0016 in $Hbb^{th3/+}$ mice could positively affect hematopoiesis and RBC lifespan and indirectly ameliorate CBC values remains to be determined.

Although ROS play an important role in cell signaling, their overproduction under pathological conditions like β-thalassemia can be associated with inflammation and injury. The observed increase in superoxide production in the liver tissues of $Hbb^{th3/+}$ mice compared to their control counterparts highlights the significant state of oxidative stress present in β-thalassemia. The increase in NADPH oxidase activity, a key enzyme complex responsible for ROS generation, further highlights the role of oxidative stress in liver pathology in $Hbb^{th3/+}$ mice. The ability of HET0016 to significantly reduce both superoxide production and NADPH oxidase activity in our study suggests that the drug exerts its protective effects by modulating oxidative stress pathways. By inhibiting 20-HETE, HET0016 likely attenuates NADPH oxidase activity, leading to a reduction in ROS levels and mitigating the downstream effects of oxidative stress on the liver. In line with our findings, other studies have also demonstrated the impact of HET0016 in decreasing intracellular ROS production and NADPH oxidase activity in the context of other diseases and across different organ systems (161). These findings paved the way for further investigation into a source of ROS that is NADPH-dependent, the CYP450.

Changes in the mRNA expression of Cyp4a10 and Cyp4a14 in mice are indicative of the upregulated CYP450 pathway. In our present study, the mRNA expression of both genes was significantly reduced in the liver following HET0016 administration. Moreover, the increased protein levels of CYP4A14 in the livers of $Hbb^{th3/+}$ mice compared to controls confirmed the dysregulation of this pathway at both the transcriptional and translational levels. The use of IHC to confirm this decrease in CYP4A expression after HET0016 treatment further validated our results. A previous study has shown the involvement and important function of CYP4A in the pathogenesis of liver conditions like nonalcoholic steatohepatitis (162). A more recent study also showed that the adminsitration of HET0016 significantly decreased the mRNA and protein expression of both Cyp4a10 and Cyp4a14 in mouse models with alcohol-induced steatosis (160). Additionally, CYP4A protein levels were found to be elevated in patients with alcoholic liver disease compared to healthy controls (160). Finally, the increased 20-HETE activity in $Hbb^{th3/+}$ mice was also aligned with the upregulation of the corresponding Cyp4a genes. The significant decrease in hepatic 20-HETE levels in $Hbb^{th3/+}$ mice following HET0016 treatment highlights the drug's potential in ameliorating the harmful effects of 20-HETE overproduction, thereby reducing liver injury. To note, only one other study to date in the context of hemoglobinopathies has implicated the role of 20-HETE in disease pathology. Vitturi et al. reported a significant upregulation of Cyp4a12a, another CYP450 enzyme responsible for 20-HETE production, in the kidneys of sickle cell disease (SCD) compared to control mice. This upregulation was linked to increased vascular congestion and renal thrombosis. Additionally, both renal CYP4A12a levels and plasma 20-HETE were significantly elevated following heme-induced acute kidney injury (AKI) in SCD mice, which correlated with enhanced expression of the renal angiotensin II receptor 1 (ATIIR1), suggesting increased vasoconstrictive activity (163).

The findings from the histological analysis performed on the liver tissues from $Hbb^{th3/+}$ mice also provided us with valuable insights into the role of HET0016 in mitigating liver injury. Firstly, H&E staining revealed signs of interstitial and perivascular inflammation, along with hepatocytic ballooning, all of which are indicative of liver damage from excess iron accumulation. These pathological features were notably improved following treatment with HET0016, suggesting that the compound can effectively target inflammatory processes in the liver. The NAS activity score further validated these improvements, highlighting the therapeutic potential of HET0016 in decreasing liver inflammation. Similarly, histological analysis with H&E staining also confirmed the protective effects of HET0016 on alcohol-induced lipid accumulation and in the liver of db/db mice in other studies (158, 160). Secondly, sirius red staining revealed signs of interstitial and perivascular fibrosis in untreated $Hbb^{th3/+}$ mice. This was significantly reduced following HET0016 administration. This reduction in fibrotic tissue is a key finding, as fibrosis is a marker of chronic liver injury, and its presence could indicate potential signs of progression to more severe liver disease conditions. Decreased mRNA expression of HGF, a marker of liver injury, in the HET0016-treated group further supported our findings on the impact of HET0016 on liver repair mechanisms. Finally, the ability of HET0016 to decrease lipid peroxidation, as shown by the significant decrease in both MDA and 4-HNE levels, is another critical finding in our study. Lipid peroxidation is a known contributor of oxidative stress and liver damage, and its attenuation suggests that HET0016 can effectively reduce oxidative damage in the liver. This reduction in oxidative stress, combined with the observed decrease in inflammation and fibrosis, points to a multifaceted protective role of HET0016 in liver pathology. The role of HET0016 in decreasing lipid peroxidation has also been previously

reported. For example, Han et al. reported lower levels in both MDA and 4-HNE content in the brain of mice 3 days after intracerebral hemorrhage and treated with HET0016 (164).

The strong association between increased oxidative stress, inflammation, and fibrosis with apoptosis and cell death in liver tissues also prompted us to look into this phenomenom. Interestingly, HET0016 significantly reduced apoptosis, as shown by both IHC and the Caspase-3 activity assay. This reduction in apoptosis is likely a direct consequence of HET0016's ability to lower oxidative stress and inflammation, which are key drivers of cell death in liver disease. Park et al. also showed that HET0016 restored the diminished insulin signaling in diabetic mice fed with HFD and rescued the increase of apoptosis in HFD livers (158). In this context, and to better understand its therpaeutic potential, future research should focus on elucidating the exact molecular mechanisms by which HET0016 modulates apoptosis in the liver, including its interactions with specific regulators and signaling molecules.

Finally, interesting findings have emerged in our in vivo study on the effect of HET0016 on iron. We assessed the effect of HET0016 on iron levels in $Hbb^{th3/+}$ mice using Perls' Prussian blue staining and measure and quantified the number of iron-positive cells. Our results demonstrated a significant decrease in liver iron content following HET0016 treatment, suggesting that HET0016 could effectively mitigate iron accumulation in the liver. Similarly, Han et al also succefully showed that HET0016 significantly reduced iron in brain sections of mice at 3 and 7 days post-intracerebral hemorrhage (164).

The reduction in iron prompted us to look into the ferroptosis pathway, a form of programmed cell death associated with iron and oxidative stress. We assessed the effects of 20-

HETE inhibition on the expression of GPX4, a key enzyme in the inhibition of ferroptosis. Our findings showed that treatment with HET0016 led to a significant increase in GPX4 expression. GPX4 plays a crucial role in protecting cells from ferroptosis by reducing lipid peroxidation, and its increased expression supports the protective effects of HET0016. Additionally, we observed that HET0016 treatment helped to preserve total glutathione levels, an important cofactor for GPX4. This preservation of GSH levels further suggests that HET0016 not only reduces iron levels but also enhances the cellular defense against ferroptosis. Similarly, Han et al also showed that 20-HETE promotes ferroptosis and that treatment with HET0016 prevcents this from happening by increasing GPX4 expression and total GSH levels (164).

Our in vivo study, while providing valuable insights, has some limitations that must be acknowledged. First, the sample size was small, which may have reduced the statistical power and generalizability of some of our findings. Second, the three study groups were very heterogenous, and not age- and sex-matched. Without proper matching, these factors may introduce some confounding variables, potentially skewing the results and limiting the ability to make definitive conclusions. Additionally, within each group itself, there was also an unequal and heterogenous distribution of animals in terms of age and sex, further complicating direct comparisons and increasing variability in the data at times. Moreover, we did not conduct a pharmacokinetic study, which limited our ability to determine the optimal dose and treatment duration of HET0016. The chosen dose and duration were based on previous studies in the literature, but this approach lacks the rigor of a tailored dosing regimen that accounts for the specific physiological characteristics of the $Hbb^{th3/+}$ mice. Another potential limitation is the method of drug administration. HET0016 was administered daily via an IP injection. The

repeated IP injections may have also contributed to increased local inflammation, which may have confounded the study's assessment of inflammation because of the treatment rather than the injection process itself. Lastly, we did not have a group of wild type/control mice treated with HET0016 to compare the effects of the drug specifically against a baseline and unaltered state, evaliuate non-specific effects, and gain insights into how the drug could impact normal physiological processes.

In light of the above-mentioned limitations, future studies should aim to address these issues by using larger, more well-matched and homogenous mouse groups, in addition to conducting a pharmacokinetic analysis to refine the dosing and consider alternative methods of drug administration such as subcutaneous injections to minimize confounding variables. Further studies in $Hbb^{th3/+}$ mice should also look at the effect of HET0016 in other organs such as a kidney and assesss the role of CYP4A in the pathogenesis of renal injury. In fact, renal renal injury is a significant complication in β-thalassemia patients and has been attributed to iron overload, chronic anemia and the use of some iron chelators (165-167). Some studies have shown that alterations in CYP4A and its metabolite 20-HETE play a key role in kidney injury in diabetic rats by upregulating TGF-β1 protein expression and levels. This increase, however, was prevented with the use of HET0016 (168). We speculate that in $Hbb^{th3/+}$ mice, CYP4A and 20-HETE production may represent a key pathophysiological mechanism driving ROS activation via TGF-β1, ultimately leading to liver cell injury. This, however, remains unknown in β-thalassemia and the signaling pathways that contribute to liver injury in $Hbb^{th3/+}$ mice warrants further investigation. Previous research has also shown that 20-HETE affects the MAPK pathway, which is associated with ferroptosis and mainly involves ERK, p38 MAPK, and c-Jun NH2-terminal

kinase (164). The exact mechanism by which HET0016 inhibits ferroptosis in $Hbb^{th3/+}$ mice requires further investigation.

Another aspect not touched upon in our in vivo study is the role of EET. Thus, a future direction for research should focus on investigating the role of EETs in the pathogenesis of liver injury in $Hbb^{th3/+}$ mice, particularly in relation to 20-HETE levels upon inhibition with HET0016. To note, EETs are known to have anti-inflammatory and vasodilatory properties (169-171). Moroever, and based on data from previous studies, 20-HETE has often been reported to play an injurious role, whereas EET have been reported to play a protective role against diabetic renal injury (172) . Moreover, there exists a cross talk between EET and 20-HETE. Given this interplay between EETs and 20-HETE in regulating oxidative stress, inflammation, and fibrosis, it would be valuable to explore how modulation of these two metabolites affects liver injury in β-thalassemia. Studying the balance between these eicosanoids could reveal even more novel insights into the mechanisms of liver damage and provide opportunities for more targeted therapeutic strategies. Finally, and since HET0016 decreased iron levels in our study, the administration of HET0016 in combination with iron chelation therapy to $Hbb^{th3/+}$ mice could represent another promising strategy to explore any potential additive or synergistic effects and further enhance a positive outcome on the liver.

In the second part of the project, we aimed to translate our findings into a clinical context by first measuring 20-HETE levels in a cohort of 50 β-thalassemia patients and 20 healthy controls. Our study, and for the first time, revealed that plasma 20-HETE levels were significantly elevated in β-thalassemia patients compared to healthy controls (p-value < 0.001). A similar study by Vittori et al in 2023 also revealed plasma 20-HETE levels to be signifcantly

elevated in SCD patients (n=9-11; $p<0.01$) compared to normal individuals (163). A sub-analysis of the data then revealed that in our cohort of β-thalassemia patients, 20-HETE levels were strongly correlated with ROS-DHE levels and exhibited a moderate correlation with iron levels. We then evaluated the impact of various treatment modalities and medications on 20-HETE levels in this patient group. Our findings indicated that 20-HETE levels were significantly higher in patients who received transfusions compared to those who did not (p-value < 0.001). Additionally, 20-HETE levels were lower in patients treated with hydroxyurea (p-value = 0.052), and those undergoing chelation therapy (p-value = 0.002). Interestingly, in patients taking at least one of the following medications: aspirin, ACE inhibitors, angiotensin II receptor blockers (ARBs), beta blockers, or insulin, 20-HETE levels were lower (p-value = 0.08). As the number of patients in our study taking one or more of these medications was very small, we were not able to stratify the patients per each medication and perform the statistical analysis. However, it is evident from the literature that these medications have an effect on 20-HETE levels. For example, ACE inhibitors can reduce the production of angiotensin II, which is known to stimulate the synthesis of 20-HETE. By inhibiting ACE, these drugs may lead to decreased levels of 20-HETE, contributing to their protective cardiovascular effects. Similarly, ARBs block the action of angiotensin II, which may also result in reduced 20-HETE production. By preventing angiotensin II from exerting its effects, ARBs can also help modulate vascular tone and improve renal function. As for aspirin, one study showed that aspirin is associated with higher levels of 20-HETE in diabetic kidney disease (173). Aspirin inhibits COX enzymes, thereby limiting the synthesis of prostaglandins and thromboxane A2. This inhibition shifts AA metabolism from the COX pathway to the CYP450 pathway, potentially leading to increased production of 20-HETE (174). Finally, insulin treatment has been shown to increase urinary 20-HETE/creatinine ratio in

patients with diabetic kidney disease ($p < 0.001$) (173). Finally, we investigated the impact of specific functional SNPs in the CYP4A and CYP4F genes on 20-HETE levels within our cohort of β-thalassemia patients. We found no significant associations between 20-HETE levels and any of the four SNPs tested (in all p value > 0.05). Similarly, Liao et al. investigated the association of four SNPs in the CYP4A and CYP4F genes (rs2269231, rs9333025, rs2108622, and rs3093135) and 20-HETE levels in 218 patients with ischemic stroke. While they found no significant associations between 20-HETE levels and any of the four variant SNPs, a stratified analysis based on different genotype combinations revealed that ischemic stroke patients carrying the genotype combination of rs9333025 GG and rs2108622 GG had higher 20-HETE levels than ischemic stroke patients with other combinations of the two variants (133). Whether the combination of different functional SNPs could affect the degree of production of 20-HETE in β-thalassemia remains to be investigated. A limitation of our study is the small sample size. A larger cohort will yield more robust and significant data. Additionally, our study groups were not fully age-matched or sex-matched, and this could have introduced variability in the results. Larger and better designed studies are needed in this context. Future research should also aim to measure both plasma and urinary 20-HETE levels. For example, the role of urinary 20-HETE as a non-invasive prognostic and diagnostic marker for diabetic kidney disease has been suggested (173). This could be relevant or of interest to look at since many β-thalassemia patients experience comorbidities such as renal dysfunction and diabetes. Investigating 20-HETE in this context could provide valuable insights into its potential as a biomarker as well. Furthermore, the effects of specific medications—such as aspirin, ACE inhibitors, ARBs, beta blockers, and insulin—on plasma and urinary 20-HETE levels in β-thalassemia patients warrant additional investigation. Finally, investigating the role of 20-HETE in endothelial cell dysfunction and

inflammation in β-thalassemia patients may hold significant promise. Given that 20-HETE is involved in the regulation of vascular tone and inflammatory responses, its dysregulation may contribute to the endothelial cell dysfunction, a phenomenom commonly observed in β-thalassemia patients (175-180). Investigating the pathways through which elevated 20-HETE levels may promote inflammatory processes and impair endothelial cell function could uncover major insights into the pathophysiology of vascular complications that are associated with β-thalassemia. Furthermore, exploring the interplay between 20-HETE and other inflammatory mediators may identify potential biomarkers for early detection and monitoring of vascular health.

CONCLUSION

In summary, our in vivo study is the first to assess the efficacy of HET0016 in reducing 20-HETE-mediated oxidative stress and injury in the livers of mice affected by β-thalassemia. The downregulation of Cyp4a10, Cyp4a14, and 20-HETE activity in $Hbb^{th3/+}$ mice with HET0016 treatment highlights the therapeutic potential of targeting the 20-HETE pathway in mitigating liver damage associated with β-thalassemia. These findings suggest that HET0016 could serve as an effective treatment strategy to alleviate liver dysfunction by modulating the dysregulated CYP450 enzymes responsible for 20-HETE production. Further research is warranted to better characterize and explore the broader implications of inhibiting this pathway in mice with β-thalassemia, in addition to its relation to the EET pathway, and its potential as a treatment for other complications of the disease. We have also showed for the first time that plasma 20-HETE levels are elevated in β-thalassemia patients compared to healthy controls. 20-HETE levels also strongly correlated with iron and ROS levels. Future research on 20-HETE in β-thalassemia patients may hold significant promise for enhancing our understanding of the disease. Investigating the role of 20-HETE as a biomarker could lead to more tailored therapeutic strategies, particularly in managing iron overload and oxidative stress. Additionally, exploring the potential influence of different SNPs on 20-HETE production may uncover new insights for clinicians. Longitudinal studies are essential to establish causal relationships and assess the impact of various treatment modalities and medications on 20-HETE levels. Ultimately, integrating these findings into clinical practice could pave the way for more effective management strategies and improved quality of life for patients with β-thalassemia.

REFERENCES

1. Kattamis A, Kwiatkowski JL, Aydinok Y. Thalassaemia. Lancet. 2022;399(10343):2310-24.
2. Taher AT, Musallam KM, Cappellini MD. β-Thalassemias. N Engl J Med. 2021;384(8):727-43.
3. Taher AT, Weatherall DJ, Cappellini MD. Thalassaemia. Lancet. 2018;391(10116):155-67.
4. Weatherall DJ. The inherited diseases of hemoglobin are an emerging global health burden. Blood. 2010;115(22):4331-6.
5. Modell B, Darlison M. Global epidemiology of haemoglobin disorders and derived service indicators. Bull World Health Organ. 2008;86(6):480-7.
6. Olivieri NF, Pakbaz Z, Vichinsky E. Hb E/beta-thalassaemia: a common & clinically diverse disorder. Indian J Med Res. 2011;134:522-31.
7. Vichinsky E. Complexity of alpha thalassemia: growing health problem with new approaches to screening, diagnosis, and therapy. Ann N Y Acad Sci. 2010;1202:180-7.
8. Lorey F, Cunningham G, Vichinsky EP, Lubin BH, Witkowska HE, Matsunaga A, et al. Universal newborn screening for Hb H disease in California. Genet Test. 2001;5(2):93-100.
9. Lorey F. Asian immigration and public health in California: thalassemia in newborns in California. J Pediatr Hematol Oncol. 2000;22(6):564-6.
10. Michlitsch J, Azimi M, Hoppe C, Walters MC, Lubin B, Lorey F, et al. Newborn screening for hemoglobinopathies in California. Pediatr Blood Cancer. 2009;52(4):486-90.
11. Angastiniotis M, Vives Corrons JL, Soteriades ES, Eleftheriou A. The impact of migrations on the health services for rare diseases in Europe: the example of haemoglobin disorders. ScientificWorldJournal. 2013;2013:727905.
12. Kattamis A, Forni GL, Aydinok Y, Viprakasit V. Changing patterns in the epidemiology of β-thalassemia. Eur J Haematol. 2020;105(6):692-703.
13. Weatherall DJ. The Evolving Spectrum of the Epidemiology of Thalassemia. Hematol Oncol Clin North Am. 2018;32(2):165-75.

14. Higgs DR, Engel JD, Stamatoyannopoulos G. Thalassaemia. Lancet. 2012;379(9813):373-83.
15. Taher AT. Thalassemia. Hematol Oncol Clin North Am. 2018;32(2):xv-xvi.
16. Tesio N, Bauer DE. Molecular Basis and Genetic Modifiers of Thalassemia. Hematol Oncol Clin North Am. 2023;37(2):273-99.
17. Mettananda S, Higgs DR. Molecular Basis and Genetic Modifiers of Thalassemia. Hematol Oncol Clin North Am. 2018;32(2):177-91.
18. Taher A, Vichinsky E, Musallam K, Cappellini M-D, Viprakasit V. Guidelines for the management of non transfusion dependent thalassaemia (NTDT): Thalassaemia International Federation, Nicosia, Cyprus; 2013.
19. Farmakis D, Porter J, Taher A, Domenica Cappellini M, Angastiniotis M, Eleftheriou A. 2021 Thalassaemia International Federation Guidelines for the Management of Transfusion-dependent Thalassemia. Hemasphere. 2022;6(8):e732.
20. Taher A. MK, Cappellini, M.D. Guidelines for the management of non-transfusion-dependent β-thalassaemia (3rd edition-2023) Thalassaemia International Federation [Available from: https://thalassaemia.org.cy/publications/tif-publications/guidelines-for-the-management-of-non-transfusion-dependent-%ce%b2-thalassaemia-3rd-edition-2023/.
21. Musallam KM, Rivella S, Vichinsky E, Rachmilewitz EA. Non-transfusion-dependent thalassemias. Haematologica. 2013;98(6):833-44.
22. Sleiman J, Tarhini A, Bou-Fakhredin R, Saliba AN, Cappellini MD, Taher AT. Non-Transfusion-Dependent Thalassemia: An Update on Complications and Management. Int J Mol Sci. 2018;19(1).
23. Bou-Fakhredin R, Motta I, Cappellini MD, Taher AT. Clinical Complications and Their Management. Hematology/Oncology Clinics. 2023;37(2):365-78.
24. Marcon A, Motta I, Taher AT, Cappellini MD. Clinical complications and their management. Hematology/Oncology Clinics. 2018;32(2):223-36.
25. Motta I, Mancarella M, Marcon A, Vicenzi M, Cappellini MD. Management of age-associated medical complications in patients with beta-thalassemia. Expert Rev Hematol. 2020;13(1):85-94.

26. Ganz T, Nemeth E. Pathogenic Mechanisms in Thalassemia II: Iron Overload. Hematology/Oncology Clinics. 2023;37(2):353-63.
27. Bou-Fakhredin R, Bazarbachi AH, Chaya B, Sleiman J, Cappellini MD, Taher AT. Iron Overload and Chelation Therapy in Non-Transfusion Dependent Thalassemia. Int J Mol Sci. 2017;18(12).
28. Berdoukas V, Nord A, Carson S, Puliyel M, Hofstra T, Wood J, et al. Tissue iron evaluation in chronically transfused children shows significant levels of iron loading at a very young age. American journal of hematology. 2013;88(11):E283-E5.
29. Borgna-Pignatti C, Meloni A, Guerrini G, Gulino L, Filosa A, Ruffo GB, et al. Myocardial iron overload in thalassaemia major. How early to check? British journal of haematology. 2014;164(4):579-85.
30. Rivella S. Iron metabolism under conditions of ineffective erythropoiesis in beta-thalassemia. Blood. 2019;133(1):51-8.
31. Taher AT, Musallam KM, El-Beshlawy A, Karimi M, Daar S, Belhoul K, et al. Age-related complications in treatment-naive patients with thalassaemia intermedia. Br J Haematol. 2010;150(4):486-9.
32. Musallam KM, Cappellini MD, Daar S, Karimi M, El-Beshlawy A, Graziadei G, et al. Serum ferritin level and morbidity risk in transfusion-independent patients with beta-thalassemia intermedia: the ORIENT study. Haematologica. 2014;99(11):e218-21.
33. Voskaridou E, Ladis V, Kattamis A, Hassapopoulou E, Economou M, Kourakli A, et al. A national registry of haemoglobinopathies in Greece: deducted demographics, trends in mortality and affected births. Annals of hematology. 2012;91:1451-8.
34. Voskaridou E, Kattamis A, Fragodimitri C, Kourakli A, Chalkia P, Diamantidis M, et al. National registry of hemoglobinopathies in Greece: updated demographics, current trends in affected births, and causes of mortality. Ann Hematol. 2019;98(1):55-66.
35. Finianos A, Matar CF, Taher A. Hepatocellular carcinoma in β-thalassemia patients: review of the literature with molecular insight into liver carcinogenesis. Int J Mol Sci. 2018;19(12):4070.

36. Taher A, Musallam KM, El Rassi F, Duca L, Inati A, Koussa S, et al. Levels of non-transferrin-bound iron as an index of iron overload in patients with thalassaemia intermedia. British journal of haematology. 2009;146(5):569-72.
37. Sikorska K, Bernat A, Wroblewska A. Molecular pathogenesis and clinical consequences of iron overload in liver cirrhosis. Hepatobiliary Pancreat Dis Int. 2016;15(5):461-79.
38. Marsella M, Ricchi P. Thalassemia and hepatocellular carcinoma: links and risks. J Blood Med. 2019;10:323-34.
39. Kohgo Y, Ikuta K, Ohtake T, Torimoto Y, Kato J. Iron overload and cofactors with special reference to alcohol, hepatitis C virus infection and steatosis/insulin resistance. World J Gastroenterol. 2007;13(35):4699-706.
40. Fibach E, Dana M. Oxidative Stress in beta-Thalassemia. Mol Diagn Ther. 2019;23(2):245-61.
41. Bou-Fakhredin R, De Franceschi L, Motta I, Eid AA, Taher AT, Cappellini MD. Redox Balance in beta-Thalassemia and Sickle Cell Disease: A Love and Hate Relationship. Antioxidants (Basel). 2022;11(5).
42. Fibach E, Rachmilewitz EA. Iron overload in hematological disorders. Presse Med. 2017;46(12 Pt 2):e296-e305.
43. Rachmilewitz EA, Weizer-Stern O, Adamsky K, Amariglio N, Rechavi G, Breda L, et al. Role of iron in inducing oxidative stress in thalassemia: Can it be prevented by inhibition of absorption and by antioxidants? Ann N Y Acad Sci. 2005;1054:118-23.
44. Pantaleo A, Giribaldi G, Mannu F, Arese P, Turrini F. Naturally occurring anti-band 3 antibodies and red blood cell removal under physiological and pathological conditions. Autoimmun Rev. 2008;7(6):457-62.
45. Rachmilewitz EA, Peisach J, Bradley TB, Blumberg WE. Role of haemichromes in the formation of inclusion bodies in haemoglobin H disease. Nature. 1969;222(5190):248-50.
46. Pantaleo A, Ferru E, Giribaldi G, Mannu F, Carta F, Matte A, et al. Oxidized and poorly glycosylated band 3 is selectively phosphorylated by Syk kinase to form large membrane clusters in normal and G6PD-deficient red blood cells. Biochem J. 2009;418(2):359-67.

47. De Franceschi L, Biondani A, Carta F, Turrini F, Laudanna C, Deana R, et al. PTPepsilon has a critical role in signaling transduction pathways and phosphoprotein network topology in red cells. Proteomics. 2008;8(22):4695-708.
48. Yuan J, Kannan R, Shinar E, Rachmilewitz EA, Low PS. Isolation, characterization, and immunoprecipitation studies of immune complexes from membranes of beta-thalassemic erythrocytes. Blood. 1992;79(11):3007-13.
49. Longo F, Piolatto A, Ferrero GB, Piga A. Ineffective Erythropoiesis in beta-Thalassaemia: Key Steps and Therapeutic Options by Drugs. Int J Mol Sci. 2021;22(13).
50. Angelucci E, Bai H, Centis F, Bafti MS, Lucarelli G, Ma L, et al. Enhanced macrophagic attack on beta-thalassemia major erythroid precursors. Haematologica. 2002;87(6):578-83.
51. Centis F, Tabellini L, Lucarelli G, Buffi O, Tonucci P, Persini B, et al. The importance of erythroid expansion in determining the extent of apoptosis in erythroid precursors in patients with beta-thalassemia major. Blood. 2000;96(10):3624-9.
52. Dussiot M, Maciel TT, Fricot A, Chartier C, Negre O, Veiga J, et al. An activin receptor IIA ligand trap corrects ineffective erythropoiesis in beta-thalassemia. Nature medicine. 2014;20(4):398-407.
53. Schrier SL, Centis F, Verneris M, Ma L, Angelucci E. The role of oxidant injury in the pathophysiology of human thalassemias. Redox Rep. 2003;8(5):241-5.
54. Semenza GL. Involvement of oxygen-sensing pathways in physiologic and pathologic erythropoiesis. Blood. 2009;114(10):2015-9.
55. Sposi NM. Oxidative stress and iron overload in β-thalassemia: an overview. Beta thalassemia. 2019;3:40-51.
56. Leecharoenkiat K, Lithanatudom P, Sornjai W, Smith DR. Iron dysregulation in beta-thalassemia. Asian Pac J Trop Med. 2016;9(11):1035-43.
57. Hershko C. Pathogenesis and management of iron toxicity in thalassemia. Ann N Y Acad Sci. 2010;1202:1-9.
58. Cabantchik ZI. Labile iron in cells and body fluids: physiology, pathology, and pharmacology. Front Pharmacol. 2014;5:45.

59. Valko M, Jomova K, Rhodes CJ, Kuca K, Musilek K. Redox- and non-redox-metal-induced formation of free radicals and their role in human disease. Arch Toxicol. 2016;90(1):1-37.
60. Bresgen N, Eckl PM. Oxidative stress and the homeodynamics of iron metabolism. Biomolecules. 2015;5(2):808-47.
61. Mancardi D, Mezzanotte M, Arrigo E, Barinotti A, Roetto A. Iron Overload, Oxidative Stress, and Ferroptosis in the Failing Heart and Liver. Antioxidants (Basel). 2021;10(12).
62. Menon AV, Tsai HP, Kim J. Cardiac iron overload promotes ferroptosis and cardiac dysfunction in mice with sickle cell disease. The FASEB Journal. 2020;34(S1):1-.
63. Menon AV, Liu J, Tsai HP, Zeng L, Yang S, Asnani A, et al. Excess heme upregulates heme oxygenase 1 and promotes cardiac ferroptosis in mice with sickle cell disease. Blood. 2022;139(6):936-41.
64. Voskou S, Aslan M, Fanis P, Phylactides M, Kleanthous M. Oxidative stress in beta-thalassaemia and sickle cell disease. Redox Biol. 2015;6:226-39.
65. Fibach E, Dana M. Oxidative stress in β-thalassemia. Molecular diagnosis & therapy. 2019;23(2):245-61.
66. Turpaev KT. Reactive oxygen species and regulation of gene expression. Biochemistry (Mosc). 2002;67(3):281-92.
67. Droge W. Free radicals in the physiological control of cell function. Physiol Rev. 2002;82(1):47-95.
68. Rahal A, Kumar A, Singh V, Yadav B, Tiwari R, Chakraborty S, et al. Oxidative stress, prooxidants, and antioxidants: the interplay. Biomed Res Int. 2014;2014:761264.
69. Blackstone NW, Kelly MM, Haridas V, Gutterman JU. Mitochondria as integrators of information in an early-evolving animal: insights from a triterpenoid metabolite. Proc Biol Sci. 2005;272(1562):527-31.
70. van der Heyde HC, Gu Y, Zhang Q, Sun G, Grisham MB. Nitric oxide is neither necessary nor sufficient for resolution of Plasmodium chabaudi malaria in mice. J Immunol. 2000;165(6):3317-23.

71. Holm E, Hildebrandt W, Kinscherf R, Droge W. Low postabsorptive net protein degradation in male cancer patients: lack of sensitivity to regulatory amino acids? Oncol Rep. 2007;17(3):695-700.
72. Scheiber MN, Watson PM, Rumboldt T, Stanley C, Wilson RC, Findlay VJ, et al. FLI1 expression is correlated with breast cancer cellular growth, migration, and invasion and altered gene expression. Neoplasia. 2014;16(10):801-13.
73. Egea J, Fabregat I, Frapart YM, Ghezzi P, Gorlach A, Kietzmann T, et al. European contribution to the study of ROS: A summary of the findings and prospects for the future from the COST action BM1203 (EU-ROS). Redox Biol. 2017;13:94-162.
74. Sies H, Cadenas E. Oxidative stress: damage to intact cells and organs. Philos Trans R Soc Lond B Biol Sci. 1985;311(1152):617-31.
75. Mullarkey CJ, Edelstein D, Brownlee M. Free radical generation by early glycation products: a mechanism for accelerated atherogenesis in diabetes. Biochem Biophys Res Commun. 1990;173(3):932-9.
76. Du G, Willet K, Mouithys-Mickalad A, Sluse-Goffart CM, Droy-Lefaix MT, Sluse FE. EGb 761 protects liver mitochondria against injury induced by in vitro anoxia/reoxygenation. Free Radic Biol Med. 1999;27(5-6):596-604.
77. Nishikawa T, Edelstein D, Brownlee M. The missing link: a single unifying mechanism for diabetic complications. Kidney Int Suppl. 2000;77:S26-30.
78. Niedowicz DM, Daleke DL. The role of oxidative stress in diabetic complications. Cell Biochem Biophys. 2005;43(2):289-330.
79. Baynes JW, Thorpe SR. Role of oxidative stress in diabetic complications: a new perspective on an old paradigm. Diabetes. 1999;48(1):1-9.
80. Wang B, Wu L, Chen J, Dong L, Chen C, Wen Z, et al. Metabolism pathways of arachidonic acids: mechanisms and potential therapeutic targets. Signal Transduct Target Ther. 2021;6(1):94.
81. Rendic S, Di Carlo FJ. Human cytochrome P450 enzymes: a status report summarizing their reactions, substrates, inducers, and inhibitors. Drug Metab Rev. 1997;29(1-2):413-580.
82. Bondy SC, Naderi S. Contribution of hepatic cytochrome P450 systems to the generation of reactive oxygen species. Biochem Pharmacol. 1994;48(1):155-9.

83. Puntarulo S, Cederbaum AI. Production of reactive oxygen species by microsomes enriched in specific human cytochrome P450 enzymes. Free Radic Biol Med. 1998;24(7-8):1324-30.
84. Fleming I, Michaelis UR, Bredenkotter D, Fisslthaler B, Dehghani F, Brandes RP, et al. Endothelium-derived hyperpolarizing factor synthase (Cytochrome P450 2C9) is a functionally significant source of reactive oxygen species in coronary arteries. Circ Res. 2001;88(1):44-51.
85. Dunn KM, Renic M, Flasch AK, Harder DR, Falck J, Roman RJ. Elevated production of 20-HETE in the cerebral vasculature contributes to severity of ischemic stroke and oxidative stress in spontaneously hypertensive rats. Am J Physiol Heart Circ Physiol. 2008;295(6):H2455-65.
86. Medhora M, Chen Y, Gruenloh S, Harland D, Bodiga S, Zielonka J, et al. 20-HETE increases superoxide production and activates NAPDH oxidase in pulmonary artery endothelial cells. Am J Physiol Lung Cell Mol Physiol. 2008;294(5):L902-11.
87. Capdevila JH, Falck JR. Biochemical and molecular characteristics of the cytochrome P450 arachidonic acid monooxygenase. Prostaglandins Other Lipid Mediat. 2000;62(3):271-92.
88. Capdevila JH, Falck JR, Harris RC. Cytochrome P450 and arachidonic acid bioactivation. Molecular and functional properties of the arachidonate monooxygenase. J Lipid Res. 2000;41(2):163-81.
89. Roman RJ, Maier KG, Sun CW, Harder DR, Alonso-Galicia M. Renal and cardiovascular actions of 20-hydroxyeicosatetraenoic acid and epoxyeicosatrienoic acids. Clin Exp Pharmacol Physiol. 2000;27(11):855-65.
90. Maier KG, Roman RJ. Cytochrome P450 metabolites of arachidonic acid in the control of renal function. Curr Opin Nephrol Hypertens. 2001;10(1):81-7.
91. Zeldin DC. Epoxygenase pathways of arachidonic acid metabolism. J Biol Chem. 2001;276(39):36059-62.
92. Powell PK, Wolf I, Jin R, Lasker JM. Metabolism of arachidonic acid to 20-hydroxy-5,8,11, 14-eicosatetraenoic acid by P450 enzymes in human liver: involvement of CYP4F2 and CYP4A11. J Pharmacol Exp Ther. 1998;285(3):1327-36.
93. Edson KZ, Rettie AE. CYP4 enzymes as potential drug targets: focus on enzyme multiplicity, inducers and inhibitors, and therapeutic modulation of 20-hydroxyeicosatetraenoic

acid (20-HETE) synthase and fatty acid ω-hydroxylase activities. Current topics in medicinal chemistry. 2013;13(12):1429-40.
94. Roman RJ. P-450 metabolites of arachidonic acid in the control of cardiovascular function. Physiol Rev. 2002;82(1):131-85.
95. Wu CC, Gupta T, Garcia V, Ding Y, Schwartzman ML. 20-HETE and blood pressure regulation: clinical implications. Cardiol Rev. 2014;22(1):1-12.
96. Fan F, Roman RJ. Effect of Cytochrome P450 Metabolites of Arachidonic Acid in Nephrology. J Am Soc Nephrol. 2017;28(10):2845-55.
97. Lasker JM, Chen WB, Wolf I, Bloswick BP, Wilson PD, Powell PK. Formation of 20-hydroxyeicosatetraenoic acid, a vasoactive and natriuretic eicosanoid, in human kidney. Role of Cyp4F2 and Cyp4A11. J Biol Chem. 2000;275(6):4118-26.
98. Bellamine A, Wang Y, Waterman MR, Gainer JV, 3rd, Dawson EP, Brown NJ, et al. Characterization of the CYP4A11 gene, a second CYP4A gene in humans. Arch Biochem Biophys. 2003;409(1):221-7.
99. Savas U, Hsu MH, Johnson EF. Differential regulation of human CYP4A genes by peroxisome proliferators and dexamethasone. Arch Biochem Biophys. 2003;409(1):212-20.
100. Kalsotra A, Strobel HW. Cytochrome P450 4F subfamily: at the crossroads of eicosanoid and drug metabolism. Pharmacol Ther. 2006;112(3):589-611.
101. Hsu MH, Savas U, Griffin KJ, Johnson EF. Human cytochrome p450 family 4 enzymes: function, genetic variation and regulation. Drug Metab Rev. 2007;39(2-3):515-38.
102. Hirani V, Yarovoy A, Kozeska A, Magnusson RP, Lasker JM. Expression of CYP4F2 in human liver and kidney: assessment using targeted peptide antibodies. Arch Biochem Biophys. 2008;478(1):59-68.
103. Zhang Y, Klaassen CD. Hormonal regulation of Cyp4a isoforms in mouse liver and kidney. Xenobiotica. 2013;43(12):1055-63.
104. Wu CC, Mei S, Cheng J, Ding Y, Weidenhammer A, Garcia V, et al. Androgen-sensitive hypertension associates with upregulated vascular CYP4A12-20-HETE synthase. J Am Soc Nephrol. 2013;24(8):1288-96.

105. Sacerdoti D, Gatta A, McGiff JC. Role of cytochrome P450-dependent arachidonic acid metabolites in liver physiology and pathophysiology. Prostaglandins Other Lipid Mediat. 2003;72(1-2):51-71.
106. Sacerdoti D, Jiang H, Gaiani S, McGiff JC, Gatta A, Bolognesi M. 11,12-EET increases porto-sinusoidal resistance and may play a role in endothelial dysfunction of portal hypertension. Prostaglandins Other Lipid Mediat. 2011;96(1-4):72-5.
107. Antoun J, Goulitquer S, Amet Y, Dreano Y, Salaun JP, Corcos L, et al. CYP4F3B is induced by PGA1 in human liver cells: a regulation of the 20-HETE synthesis. J Lipid Res. 2008;49(10):2135-41.
108. Plee-Gautier E, Antoun J, Goulitquer S, Le Jossic-Corcos C, Simon B, Amet Y, et al. Statins increase cytochrome P450 4F3-mediated eicosanoids production in human liver cells: a PXR dependent mechanism. Biochem Pharmacol. 2012;84(4):571-9.
109. Sacerdoti D, Balazy M, Angeli P, Gatta A, McGiff JC. Eicosanoid excretion in hepatic cirrhosis. Predominance of 20-HETE. J Clin Invest. 1997;100(5):1264-70.
110. Li B, Ma Y, Tan L, Ren H, Wu L, Su Q, et al. 20-Hydroxytetraenoic acid induces hepatic fibrosis via the TGF-beta1/Smad3 signaling pathway. Toxicol Lett. 2023;373:1-12.
111. Bou-Fakhredin R, Rivella S, Cappellini MD, Taher AT. Pathogenic Mechanisms in Thalassemia I: Ineffective Erythropoiesis and Hypercoagulability. Hematol Oncol Clin North Am. 2023;37(2):341-51.
112. Taher AT, Cappellini MD, Bou-Fakhredin R, Coriu D, Musallam KM. Hypercoagulability and Vascular Disease. Hematol Oncol Clin North Am. 2018;32(2):237-45.
113. Hoopes SL, Garcia V, Edin ML, Schwartzman ML, Zeldin DC. Vascular actions of 20-HETE. Prostaglandins Other Lipid Mediat. 2015;120:9-16.
114. Ishizuka T, Cheng J, Singh H, Vitto MD, Manthati VL, Falck JR, et al. 20-Hydroxyeicosatetraenoic acid stimulates nuclear factor-kappaB activation and the production of inflammatory cytokines in human endothelial cells. J Pharmacol Exp Ther. 2008;324(1):103-10.
115. Garcia V, Gilani A, Shkolnik B, Pandey V, Zhang FF, Dakarapu R, et al. 20-HETE signals through G-protein–coupled receptor GPR75 (Gq) to affect vascular function and trigger hypertension. Circulation research. 2017;120(11):1776-88.

116. Pascale JV, Park EJ, Adebesin AM, Falck JR, Schwartzman ML, Garcia V. Uncovering the signalling, structure and function of the 20-HETE-GPR75 pairing: Identifying the chemokine CCL5 as a negative regulator of GPR75. Br J Pharmacol. 2021;178(18):3813-28.
117. Zeng Q, Han Y, Bao Y, Li W, Li X, Shen X, et al. 20-HETE increases NADPH oxidase-derived ROS production and stimulates the L-type Ca2+ channel via a PKC-dependent mechanism in cardiomyocytes. Am J Physiol Heart Circ Physiol. 2010;299(4):H1109-17.
118. Regner KR, Zuk A, Van Why SK, Shames BD, Ryan RP, Falck JR, et al. Protective effect of 20-HETE analogues in experimental renal ischemia reperfusion injury. Kidney Int. 2009;75(5):511-7.
119. Hoff U, Lukitsch I, Chaykovska L, Ladwig M, Arnold C, Manthati VL, et al. Inhibition of 20-HETE synthesis and action protects the kidney from ischemia/reperfusion injury. Kidney Int. 2011;79(1):57-65.
120. Yu W, Chen L, Yang YQ, Falck JR, Guo AM, Li Y, et al. Cytochrome P450 omega-hydroxylase promotes angiogenesis and metastasis by upregulation of VEGF and MMP-9 in non-small cell lung cancer. Cancer Chemother Pharmacol. 2011;68(3):619-29.
121. Shastry BS. SNP alleles in human disease and evolution. J Hum Genet. 2002;47(11):561-6.
122. Nahon P, Zucman-Rossi J. Single nucleotide polymorphisms and risk of hepatocellular carcinoma in cirrhosis. J Hepatol. 2012;57(3):663-74.
123. Dwi Astarini F, Ratnasari N, Wasityastuti W. Update on Non-Alcoholic Fatty Liver Disease-Associated Single Nucleotide Polymorphisms and Their Involvement in Liver Steatosis, Inflammation, and Fibrosis: A Narrative Review. Iran Biomed J. 2022;26(4):252-68.
124. Villicana S, Bell JT. Genetic impacts on DNA methylation: research findings and future perspectives. Genome Biol. 2021;22(1):127.
125. Kerkel K, Spadola A, Yuan E, Kosek J, Jiang L, Hod E, et al. Genomic surveys by methylation-sensitive SNP analysis identify sequence-dependent allele-specific DNA methylation. Nat Genet. 2008;40(7):904-8.
126. Hatton AA, Cheng FF, Lin T, Shen RJ, Chen J, Zheng Z, et al. Genetic control of DNA methylation is largely shared across European and East Asian populations. Nat Commun. 2024;15(1):2713.

127. Jarrar YB, Lee SJ. Molecular Functionality of Cytochrome P450 4 (CYP4) Genetic Polymorphisms and Their Clinical Implications. Int J Mol Sci. 2019;20(17).
128. Sirotina S, Ponomarenko I, Kharchenko A, Bykanova M, Bocharova A, Vagaytseva K, et al. A Novel Polymorphism in the Promoter of the CYP4A11 Gene Is Associated with Susceptibility to Coronary Artery Disease. Dis Markers. 2018;2018:5812802.
129. Yan H, Yuan Y, Zhang P, Huang Z, Chang L, Gui Y. CYP4F2 gene single nucleotide polymorphism is associated with ischemic stroke. Genet Mol Res. 2015;14(1):659-64.
130. Fava C, Montagnana M, Almgren P, Rosberg L, Lippi G, Hedblad B, et al. The V433M variant of the CYP4F2 is associated with ischemic stroke in male Swedes beyond its effect on blood pressure. Hypertension. 2008;52(2):373-80.
131. Gainer JV, Bellamine A, Dawson EP, Womble KE, Grant SW, Wang Y, et al. Functional variant of CYP4A11 20-hydroxyeicosatetraenoic acid synthase is associated with essential hypertension. Circulation. 2005;111(1):63-9.
132. Mayer B, Lieb W, Gotz A, Konig IR, Aherrahrou Z, Thiemig A, et al. Association of the T8590C polymorphism of CYP4A11 with hypertension in the MONICA Augsburg echocardiographic substudy. Hypertension. 2005;46(4):766-71.
133. Liao D, Yi X, Zhang B, Zhou Q, Lin J. Interaction between CYP4F2 rs2108622 and CPY4A11 rs9333025 variants is significantly correlated with susceptibility to ischemic stroke and 20-hydroxyeicosatetraenoic acid level. Genetic testing and molecular biomarkers. 2016;20(5):223-8.
134. Ward NC, Tsai I-J, Barden A, van Bockxmeer FM, Puddey IB, Hodgson JM, et al. A single nucleotide polymorphism in the CYP4F2 but not CYP4A11 gene is associated with increased 20-HETE excretion and blood pressure. Hypertension. 2008;51(5):1393-8.
135. Lino Cardenas CL, Renault N, Farce A, Cauffiez C, Allorge D, Lo-Guidice JM, et al. Genetic polymorphism of CYP4A11 and CYP4A22 genes and in silico insights from comparative 3D modelling in a French population. Gene. 2011;487(1):10-20.
136. Hiratsuka M, Nozawa H, Katsumoto Y, Moteki T, Sasaki T, Konno Y, et al. Genetic polymorphisms and haplotype structures of the CYP4A22 gene in a Japanese population. Mutat Res. 2006;599(1-2):98-104.

137. Bou-Fakhredin R, Dia B, Ghadieh HE, Rivella S, Cappellini MD, Eid AA, et al. CYP450 Mediates Reactive Oxygen Species Production in a Mouse Model of beta-Thalassemia through an Increase in 20-HETE Activity. Int J Mol Sci. 2021;22(3).
138. Fernandes DC, Wosniak J, Jr., Pescatore LA, Bertoline MA, Liberman M, Laurindo FR, et al. Analysis of DHE-derived oxidation products by HPLC in the assessment of superoxide production and NADPH oxidase activity in vascular systems. Am J Physiol Cell Physiol. 2007;292(1):C413-22.
139. Fernandes DC, Goncalves RC, Laurindo FR. Measurement of Superoxide Production and NADPH Oxidase Activity by HPLC Analysis of Dihydroethidium Oxidation. Methods Mol Biol. 2017;1527:233-49.
140. Haddad M, Eid S, Harb F, Massry MEL, Azar S, Sauleau EA, et al. Activation of 20-HETE Synthase Triggers Oxidative Injury and Peripheral Nerve Damage in Type 2 Diabetic Mice. J Pain. 2022;23(8):1371-88.
141. Cao Y, Yang H, Huang Y, Lu J, Du H, Wang B. Mesenchymal stem cell-derived exosomal miR-26a induces ferroptosis, suppresses hepatic stellate cell activation, and ameliorates liver fibrosis by modulating SLC7A11. Open Med (Wars). 2024;19(1):20240945.
142. Qiu L, Yan Y, Zhong G, Hou Z, Ye Y, Lin J, et al. Hydromorphone hydrochloride preconditioning combined with postconditioning attenuates myocardial ischemia/reperfusion injury in rats by improving mitochondrial function and activating the PI3K/Akt signaling pathway. Chem Biol Drug Des. 2024;103(2):e14474.
143. Hu B, Zhang XX, Zhang T, Yu WC. Dissecting molecular mechanisms underlying ferroptosis in human umbilical cord mesenchymal stem cells: Role of cystathionine gamma-lyase/hydrogen sulfide pathway. World J Stem Cells. 2023;15(11):1017-34.
144. Wang X, Li M, Diao K, Wang Y, Chen H, Zhao Z, et al. Deferoxamine attenuates visual impairment in retinal ischemia–reperfusion via inhibiting ferroptosis. Sci Rep. 2023;13(1):20145.
145. Wang J, Jia Q, Jiang S, Lu W, Ning H. POU6F1 promotes ferroptosis by increasing lncRNA-CASC2 transcription to regulate SOCS2/SLC7A11 signaling in gastric cancer. Cell Biol Toxicol. 2024;40(1):3.

146. Wang X, Shen T, Lian J, Deng K, Qu C, Li E, et al. Resveratrol reduces ROS-induced ferroptosis by activating SIRT3 and compensating the GSH/GPX4 pathway. Mol Med. 2023;29(1):137.
147. Shivling Mali A, Honc O, Hejnova L, Novotny J. Opioids Alleviate Oxidative Stress via the Nrf2/HO-1 Pathway in LPS-Stimulated Microglia. Int J Mol Sci. 2023;24(13).
148. Hwangbo H, Park C, Bang E, Kim HS, Bae SJ, Kim E, et al. Morroniside Protects C2C12 Myoblasts from Oxidative Damage Caused by ROS-Mediated Mitochondrial Damage and Induction of Endoplasmic Reticulum Stress. Biomol Ther (Seoul). 2024;32(3):349-60.
149. Li P, Cao G. PDCD4 silencing alleviates KA-induced neurotoxicity of HT22 cells by inhibiting endoplasmic reticulum stress via blocking the MAPK/NF-kappaB signaling pathway. Exp Ther Med. 2024;27(2):55.
150. Costantino S, Mengozzi A, Velagapudi S, Mohammed SA, Gorica E, Akhmedov A, et al. Treatment with recombinant Sirt1 rewires the cardiac lipidome and rescues diabetes-related metabolic cardiomyopathy. Cardiovasc Diabetol. 2023;22(1):312.
151. Nizar R, Cazacu S, Xiang C, Krasner M, Barbiro-Michaely E, Gerber D, et al. Propofol Inhibits Glioma Stem Cell Growth and Migration and Their Interaction with Microglia via BDNF-AS and Extracellular Vesicles. Cells. 2023;12(15).
152. Montilla-Lopez P, Munoz-Agueda MC, Feijoo Lopez M, Munoz-Castaneda JR, Bujalance-Arenas I, Tunez-Finana I. Comparison of melatonin versus vitamin C on oxidative stress and antioxidant enzyme activity in Alzheimer's disease induced by okadaic acid in neuroblastoma cells. Eur J Pharmacol. 2002;451(3):237-43.
153. Janciauskiene S, Ahren B. Fibrillar islet amyloid polypeptide differentially affects oxidative mechanisms and lipoprotein uptake in correlation with cytotoxicity in two insulin-producing cell lines. Biochemical and biophysical research communications. 2000;267(2):619-25.
154. Mattson JP, Sun J, Murray DM, Poole DC. Lipid peroxidation in the skeletal muscle of hamsters with emphysema. Pathophysiology. 2002;8(3):215-21.
155. Knudsen LRV, Karstrup CC, Pedersen HG, Agerholm JS, Jensen TK, Klitgaard K. Revisiting bovine pyometra—New insights into the disease using a culture-independent deep sequencing approach. Veterinary microbiology. 2015;175(2-4):319-24.

156. Colosimo A, Gatta V, Guida V, Leodori E, Foglietta E, Rinaldi S, et al. Application of MLPA assay to characterize unsolved alpha-globin gene rearrangements. Blood Cells Mol Dis. 2011;46(2):139-44.
157. Garm Spindler KL, Pallisgaard N, Rasmussen AA, Lindebjerg J, Andersen RF, Cruger D, et al. The importance of KRAS mutations and EGF61A>G polymorphism to the effect of cetuximab and irinotecan in metastatic colorectal cancer. Ann Oncol. 2009;20(5):879-84.
158. Park EC, Kim SI, Hong Y, Hwang JW, Cho GS, Cha HN, et al. Inhibition of CYP4A reduces hepatic endoplasmic reticulum stress and features of diabetes in mice. Gastroenterology. 2014;147(4):860-9.
159. Hashemizadeh H, Noori R, Kolagari S. Assessment Hepatomegaly and liver Enzymes in 100 Patients with beta Thalassemia Major in Mashhad, Iran. Iran J Ped Hematol Oncol. 2012;2(4):171-7.
160. Yang Z, Smalling RV, Huang Y, Jiang Y, Kusumanchi P, Bogaert W, et al. The role of SHP/REV-ERBalpha/CYP4A axis in the pathogenesis of alcohol-associated liver disease. JCI Insight. 2021;6(16).
161. Alaeddine LM, Harb F, Hamza M, Dia B, Mogharbil N, Azar NS, et al. Pharmacological regulation of cytochrome P450 metabolites of arachidonic acid attenuates cardiac injury in diabetic rats. Transl Res. 2021;235:85-101.
162. Zhang X, Li S, Zhou Y, Su W, Ruan X, Wang B, et al. Ablation of cytochrome P450 omega-hydroxylase 4A14 gene attenuates hepatic steatosis and fibrosis. Proc Natl Acad Sci U S A. 2017;114(12):3181-5.
163. Vitturi D, Crosby D, Lenhart SC, Carreno M, Lenhart D, Ghosh S. 20-HETE As an Emerging Target to Improve Renal Health in Sickle Cell Disease. Blood. 2023;142:3857.
164. Han R, Wan J, Han X, Ren H, Falck JR, Munnuri S, et al. 20-HETE Participates in Intracerebral Hemorrhage-Induced Acute Injury by Promoting Cell Ferroptosis. Front Neurol. 2021;12:763419.
165. Demosthenous C, Vlachaki E, Apostolou C, Eleftheriou P, Kotsiafti A, Vetsiou E, et al. Beta-thalassemia: renal complications and mechanisms: a narrative review. Hematology. 2019;24(1):426-38.

166. Mallat NS, Musallam KM, Mallat SG, Ziyadeh FN, Koussa S, Taher AT. End stage renal disease in six patients with beta-thalassemia intermedia. Blood Cells Mol Dis. 2013;51(3):146-8.
167. Mallat NS, Mallat SG, Musallam KM, Taher AT. Potential mechanisms for renal damage in beta-thalassemia. J Nephrol. 2013;26(5):821-8.
168. Eid S, Abou-Kheir W, Sabra R, Daoud G, Jaffa A, Ziyadeh F, et al. Involvement of renal cytochromes P450 and arachidonic acid metabolites in diabetic nephropathy. Journal of biological regulators and homeostatic agents. 2013;27(3):693-703.
169. Node K, Huo Y, Ruan X, Yang B, Spiecker M, Ley K, et al. Anti-inflammatory properties of cytochrome P450 epoxygenase-derived eicosanoids. Science. 1999;285(5431):1276-9.
170. Campbell WB. New role for epoxyeicosatrienoic acids as anti-inflammatory mediators. Trends Pharmacol Sci. 2000;21(4):125-7.
171. Zeldin DC, Liao JK. Reply: cytochrome P450-derived eicosanoids and the vascular wall. Trends Pharmacol Sci. 2000;21(4):127-8.
172. Luo Y, Wu MY, Deng BQ, Huang J, Hwang SH, Li MY, et al. Inhibition of soluble epoxide hydrolase attenuates a high-fat diet-mediated renal injury by activating PAX2 and AMPK. Proc Natl Acad Sci U S A. 2019;116(11):5154-9.
173. Houeiss P, Njeim R, Tamim H, Hamdy AF, Azar TS, Azar WS, et al. Urinary 20-HETE: A prospective Non-Invasive prognostic and diagnostic marker for diabetic kidney disease. J Adv Res. 2023;44:109-17.
174. Liu JY, Yang J, Inceoglu B, Qiu H, Ulu A, Hwang SH, et al. Inhibition of soluble epoxide hydrolase enhances the anti-inflammatory effects of aspirin and 5-lipoxygenase activation protein inhibitor in a murine model. Biochem Pharmacol. 2010;79(6):880-7.
175. Stoyanova E, Trudel M, Felfly H, Lemsaddek W, Garcia D, Cloutier G. Vascular endothelial dysfunction in beta-thalassemia occurs despite increased eNOS expression and preserved vascular smooth muscle cell reactivity to NO. PLoS One. 2012;7(6):e38089.
176. Kheansaard W, Phongpao K, Paiboonsukwong K, Pattanapanyasat K, Chaichompoo P, Svasti S. Microparticles from beta-thalassaemia/HbE patients induce endothelial cell dysfunction. Sci Rep. 2018;8(1):13033.

177. Aggeli C, Antoniades C, Cosma C, Chrysohoou C, Tousoulis D, Ladis V, et al. Endothelial dysfunction and inflammatory process in transfusion-dependent patients with beta-thalassemia major. Int J Cardiol. 2005;105(1):80-4.
178. El-Kinawy NS, Andrawes NG. Endothelial and peripheral blood cell activation in β-thalassemia children. The Egyptian Journal of Haematology. 2012;37(3):156-61.
179. Cheung YF, Chan GC, Ha SY. Arterial stiffness and endothelial function in patients with beta-thalassemia major. Circulation. 2002;106(20):2561-6.
180. Morris CR. Mechanisms of vasculopathy in sickle cell disease and thalassemia. Hematology Am Soc Hematol Educ Program. 2008:177-85.